University of Crete

Department of Biology

Postgraduate program in Protein Biotechnology

MSc thesis

Engineering an (*R*)-selective amine transaminase for the acceptance of bulky substrates

By Eleni Konia

Committee:

Assist. Prof. Dr. Ioannis Pavlidis (supervisor)

Prof. Dr. Georgios Tsiotis

Assoc. Prof. Dr. Francesco Mutti

Heraklion, January 2022

Supervisor:

Dr. Ioannis Pavlidis

Assist. Prof. of Biological Chemistry, Department of Chemistry, University of Crete, GR

Examining Committee:

Dr. Georgios Tsiotis

Prof. of Structure and Function of Proteins, Department of Chemistry, University of Crete, GR

Dr. Francesco Mutti

Assoc. Professor of Biocatalysis, Van´t Hoff Institute for Molecular Sciences, University of Amsterdam, NL

Table of contents

Acknowledgements

I want to thank Prof. I. Pavlidis for always giving the most of his support and guidance to all of us. Despite the workload you always kept constant track of the development of every student and worked hard so that we could have every opportunity possible. Moreover, the shelf with the tokens of collective failed experiments will not only make us laugh, but it is also a reminder that you supported us even when we (occasionally) failed.

Moving on, Vasili every single organic reaction scheme in the thesis is for you, Thomai I am so glad that we went through this master's program together and Chara I will always stand amazed in front your unbelievable set of skills. I remember the first day I met each one of you, you 've been great friends and the best lab mates I could ever wish for. I also want to thank Nikos for all the great time we spend trying to figure out the GC, Malvina for being awesome and Konstantinos for the great cooperation. Moreover, I want to collectively thank all the students of the biochemistry department for being so fun, kind and always willing to help. I also owe a long delayed thanks to former lab members Anna and Serpil. Lastly, this thesis is dedicated to Mrs. Kavelaki, an amazing biochemistry teacher.

A solid knowledge of the structure of the enzyme was essential to this work and I want to thank Prof. Tsiotis and his collaborators, A. Drakonaki, C. Muenke and Dr. U. Ermler for experimentally elucidating the three-dimensional structure of the amine transaminase form *Luminiphilus syltensis.* I am also grateful to Prof. Tsiotis, my supervisor Prof. Pavlidis and Prof. Mutti for taking the time and effort to review this work.

This MSc thesis was supported by the Hellenic Foundation for Research and Innovation (H.F.R.I.) under the "1st Call for H.F.R.I. Research Projects to support Faculty Members & Researchers and the Procurement of High-Cost Research Equipment Grant" (Project Number:664).

Abstract

Amine transaminases catalyze the transfer of an amino group from a primary amine (amino donor) to the carbonyl carbon of an α-keto acid, a ketone or an aldehyde (amine acceptor). The process of amine transfer is called transamination. The reaction is mediated by an organic cofactor, pyridoxal 5'-phosphate (PLP). Because of the industrial potential of ATAs for production of chiral amines, many research efforts have been devoted to improve the catalytic activity of the ATAs. Optically pure amines are valuable products or intermediate compounds for the synthesis of pharmaceuticals and agrochemicals. While amine transaminases are highly enantioselective catalysts, they only accept methyl substituted phenylamines due to the architecture of their active site. This thesis focuses on engineering the substrate scope of an (*R*)-selective amine transaminase form *Luminiphilus syltensis* (LS_ATA) towards alkyl substituted amines. A structure-based rational design strategy was implemented starting from a high-resolution crystallographic structure of the LS_ATA that was resolved by our collaborators. We prepared *in silico,* through MD simulations, the quinonoid intermediate of (*R*)-1-phenylethylamine, which is a benchmark substrate of amine transaminases. The model of the intermediate helped us gain insight on important structural features in the enzymes active and binding site. Through bioinformatic analysis and visual inspection we identified three residues in the enzyme's small binding pocket that possibly hinder the acceptance of bulkier substrates. Site directed mutagenesis confirmed that the mutation V37A in the small binding pocket generates a variant with expanded substrate scope toward bulkier compounds, without any loss in enantioselectivity and enzyme stability. The resulting variant successfully deaminated (*R*)-1-phenylpropylamine and (*R*)-1-phenylbutylamine, however no asymmetric synthesis of these amines was observed. Mutation in positions S248A and T249A led to deactivation of the enzymes, mainly owe to unreactive complexes between the enzyme and the PLP cofactor.

Part of the thesis was published in the following article:

Konia E, Chatzicharalampous K, Drakonaki A, Muenke C, Ermler U, Tsiotis G, Pavlidis IV. Rational engineering of *Luminiphilus syltensis* (*R*)-selective amine transaminase for the acceptance of bulky substrates. Chem Comm. 2021, 57(96) 12948-12951.

Περίληψη

Τρανσαμινάσες ή αμινοτρανσφεράσες ονομάζονται τα ένζυμα που καταλύουν αντιδράσεις απαμίνωσης αμινοξέων ή πρωτοταγών αμινών (δότης) προς σχηματισμό της αντίστοιχης καρβονυλικής ένωσης. Η αμινομάδα που διασπάται μεταφέρεται σε μια δεύτερη καρβονυλική ένωση (δέκτης) σχηματίζοντας μια νέα αμίνη ή αμινοξύ. Στην μεταφορά της αμινομάδας μεταξύ των δύο ενώσεων συμμετέχει ο συμπαράγοντας φωσφορικής πυριδοξάλης (PLP). Οι ενζυμικά καταλυώμενες αντιδράσεις τρανσαμίνωσης πλεονεκτούν σε σχέση με άλλες αντιδράσεις σύνθεσης αμινών καθώς η αντίδραση πραγματοποιείται εναντιοεκλεκτικά. Ιδιαίτερα οι τρανσαμινάσες πρωτοταγών αμινών έχουν βρει εφαρμογή στη βιομηχανία για την παραγωγή οπτικά καθαρών αμινών που αποτελούν πρόδρομες ενώσεις φαρμάκων ή αγροχημικών. Τα ένζυμα αυτά μπορούν να χρησιμοποιηθούν ως καταλύτες, είτε με σκοπό τον κινητικό διαχωρισμό ρακεμικών μειγμάτων πρωτοταγών αμινών, είτε για την ασύμμετρη σύνθεση χειρόμορφων αμινών από προχειρόμορφες κετόνες ή αλδεΰδες. Στο ενεργό τους κέντρο, οι τρανσαμινάσες διαθέτουν δύο κοιλότητες, η κάθε μια από τις οποίες δρα ως θέση πρόσδεσης του ενός από τους δυο υποκαταστάτες της χειρόμορφης πρωτοταγούς αμίνης ή της προχειρόμορφης καρβονυλικής ένωσης. Επειδή διαφέρουν σε μέγεθος, είναι γνωστές ως η μεγάλη και η μικρή θέση πρόσδεσης. Χάρη σε αυτή την αρχιτεκτονική τα υποστρώματα προσδένονται με αυστηρή γεωμετρία γεγονός που εξασφαλίζει την εναντιοεκλεκτικότητα της αντίδρασης. Ωστόσο συχνά παρατηρείται ότι η μικρή θέση δεν μπορεί να προσδέσει υποκαταστάτες μεγαλύτερους της αίθυλο-ομάδας. Σκοπός της παρούσας εργασίας είναι ο λογικός ανασχεδιασμός της (*R*)-εναντιοεκλεκτικής τρανσαμινάσης από τον οργανισμό *Luminiphilus syltensis* (LS_ATA). Ξεκινώντας από την κρυσταλλική δομή του ενζύμου δημιουργήσαμε ένα μοντέλο της πρωτεΐνης σε μια από τις ενδιάμεσες καταστάσεις του συμπλόκου PLP-υποστρώματος από την οποία διέρχεται η αντίδραση πριν οδηγηθεί σε προϊόν. Η ενδιάμεση αυτή κατάσταση είναι γνωστή ως κινονοειδές ενδιάμεσο και δημιουργήθηκε μέσω της μεθόδου μοριακής δυναμικής προσομοίωσης. Ως υπόστρωμα χρησιμοποιήθηκε η (*R*)-1-φαινυλεθυλαμινη (υπόστρωμα αναφοράς). Στη συνέχεια επεκτείναμε *in silico* τον άλκυλο υποκαταστάτη του υποστρώματος στη μικρή θέση πρόσδεσης. Τρία αμινοξικά κατάλοιπα της μικρής θέσης πρόσδεσης (V37, S248, T249) επιλέχθηκαν για μεταλλαξιγένεση. Το μετάλλαγμα V37A χρησιμοποιήθηκε σε μικρής κλίμακας αντιδράσεις και παρουσίασε δραστικότητα ως προς την (*R*)-1-φαινυλβουτυλαμίνη η οποία δεν γίνεται δεκτή από το φυσικού τύπου ένζυμο. Μεταλλαγή των θέσεων 248 και 249 οδηγεί σε λιγότερο ή καθόλου ενεργά ανασυνδιασμένα ένζυμα. Η παρουσία

πολικών αμινοξέων στις θέσεις αυτές είναι μάλλον καθοριστική για την πρόσδεση του συμπαράγοντα.

Μέρος της παρούσας εργασίας δημοσιεύτηκε στο εξής άρθρο:

Konia E, Chatzicharalampous K, Drakonaki A, Muenke C, Ermler U, Tsiotis G, Pavlidis IV. Rational engineering of *Luminiphilus syltensis* (*R*)-selective amine transaminase for the acceptance of bulky substrates. *Chem Comm*. 2021, 57(96) 12948-12951.

Abbreviations

ATA	amine transaminase
LS_ATA	*Luminiphilus syltensis* ATA
(*R*)-ATA	(*R*)-selective ATA
(*S*)-ATA	(*S*)-selective ATA
α-TA	α-amino acid transaminase
ω-TA	ω-amino acid transaminase
ADCL	amino deoxychorismate lyase
BCAT	branched-chain amino acid transaminase
CATH	protein secondary structure database
DAAT	D-amino acid transaminase
DMSO	dimethyl sulfoxide
ee_s	enantiomeric excess of the substrate
FID	flame ionization detector
GC	gas chromatography
GDH	glucose dehydrogenase
IPA	isopropylamine
LDH	lactate dehydrogenase
MD	molecular dynamic
NCBI	national center for biotechnology information
OD_{600}	optical density at 600 nm
PLP	pyridoxal 5'-phosphate
PMP	pyridoxamine 5'-phosphate
PEA	1-phenylethylamine
PPA	1-phenylpropylamine
PBA	1-phenylbutylamine
PDB	protein data bank
RMSD	root-mean-square deviation
U	enzyme activity unit
WT	wild-type

CHAPTER 1

Introduction

1.1 Transaminases nomenclature

In living cells, transaminases participate in the metabolism of amino acids or amino containing compounds. The reaction always involves the transfer of an amino group from an amino donor (e.g., amino acid, amine) to an amino acceptor molecule that contains a carbonyl group (e.g., α-keto acid, ketone or aldehyde). It is common practice to name transaminases (E.C. 2.6.1.x) based on the amino donor compounds that they bind.[1] Transaminases that are active against α-amino acids are called α-amino acid transaminases (α-TAs). Another group of transaminases can transfer amine groups other than the α-amino group of amino acids, for example the δ-amino group in ornithine or the γ-amino group in γ-aminobutyric acid and are collectively referred to as ω-transaminases (ω-TAs). A subgroup of ω-TAs, amine transaminases (ATAs), show high reactivity towards primary amines.[2] ATAs have been extensively studied due to their industrial application in the synthesis of pharmaceuticals and agrochemicals.[3,4] Amine transaminases exhibit a preference for either the (*S*)- or (*R*)-enantiomer of primary amines ((*R*)-ATAs and (*S*)-ATAs, respectively).

1.2 Amine transaminases, a class of PLP-dependent enzymes

Amine transaminases (ATAs) belong in the family of PLP-dependent enzymes. The pyridoxal 5'-phosphate (PLP) cofactor, a Vitamin B_6 derivative, acts in association with many apoenzymes to catalyze reactions concerning amino acids or amino-containing metabolites.[5] Various enzymatic activities can be found in the family of PLP dependent enzymes. It is worth noting that PLP-dependent enzymes can be found in 5 out of the 7 categories.[6]

The different catalytic functions of PLP-dependent enzymes correlate with the differences between the enzyme tertiary structures. Different spatial organizations of the ligand binding sites and the cofactor orientation lead to different reaction mechanisms. Seven topological families (fold types I-VII) have been identified,[7] on the basis of the - so far known - crystallographic structures. Enzymes that belong to same fold type share a similar

overall shape, connectivity of secondary structure elements and sometimes conserved amino acid residues. Shared topology does not necessarily imply any evolutionary connection, however common evolutionary origins of PLP-depended enzymes have been suggested.[8] PLP-dependent enzymes with transamination activity belong to fold types I and IV. All (*R*)-ATAs reported so far belong to fold type IV,[9] while (*S*)-ATAs belong to fold type I.[10] Two other enzyme families share the structural fold of (*R*)-ATAs:

- D-amino acid transaminases (DAATs) which are selective for D-α-amino acids like D-alanine and D-glutamate, which are constituents of bacterial cell walls.[9,11]
- L-branched-chain amino acid transaminases (BCATs) which participate in the metabolism of the amino acids L-valine, L-leucine and L-isoleucine.[12]

Even though they share the same tertiary structure fold, BCATs have a different enantiopreference compared to DAATs and (*R*)-ATAs. Amino lyases active towards 4-amino-4-deoxychorismate (ADCLs)[13] have also been classified as fold type IV enzymes.

1.3 Quaternary structure of the amine transaminase from *Luminiphilus syltensis*

As expected for fold type IV enzymes, the (*R*)-selective amine transaminase from *Luminiphilus syltensis* (LS_ATA) is a homomultimeric protein (**Figure 1**).[9] Six polypeptide chains are organized in three homodimers which further assemble in a hexameric structure. The crystallographic structure (1.6 Å resolution) was elucidated in collaboration with the group of Prof. Tsiotis and their partners in Max Planck Institute in Frankfurt. They also verified that the enzyme exists only in hexameric form in solution, through gel filtration experiments.[14]

The structure of one out of the three homodimers is shown in **Figure 2.** The peptide chain of each subunit folds into two domains. The N-terminal domain (residues 1-119) has an α/β sandwich motif and the C-terminal domain (residues 128- 295) has an α/β barrel structure. An interdomain loop (residues 120-127) connects the two domains.

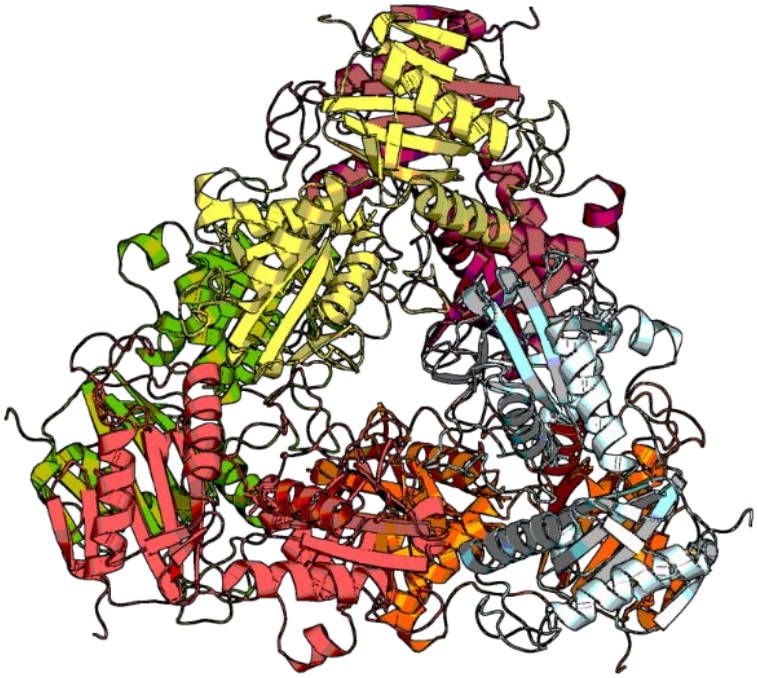

Figure 1. Quaternary structure of the hexameric (trimer of dimers) form of the (*R*)-ATA from *Luminiphilus syltensis* (PDB code 7p3t). A different color is applied to each monomer. Modified from Konia et al.,[14] use via creative commons license.

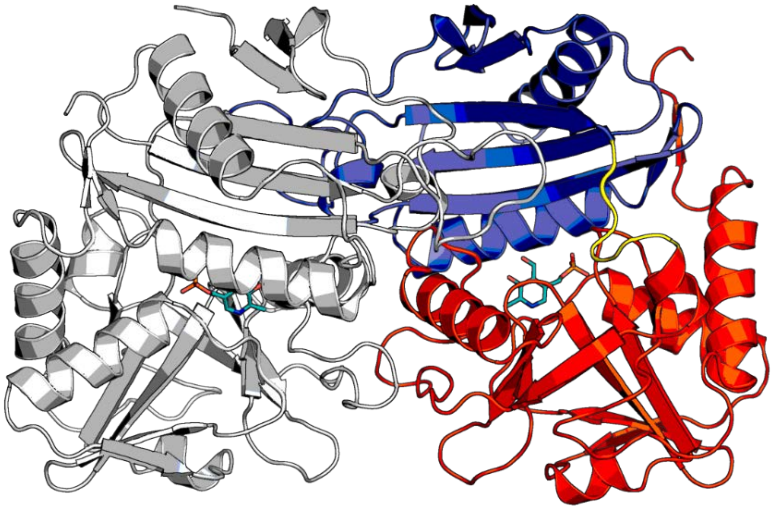

Figure 2. Ribbon view of the homodimeric complex of the (*R*)-ATA from *Luminiphilus syltensis* (PDB code 7p3t). One PLP molecule is coordinated in the active site of each subunit and shown in sticks. The first subunit is colored white. In the second subunit the N-terminal domain is colored blue (α/β sandwich motif) and the C-terminal domain is colored red (α/β barrel structure). The interdomain loop is colored yellow. The overall fold is typical for fold type IV PLP-dependent enzymes.

1.4 Coordination of the cofactor and the substrates

The active site of the transaminase consists of the cofactor coordination pocket, the binding pockets of the substrates and provides the environment where the chemical transformation occurs (section 1.6). Even though transaminases of fold type IV arrange in tetramers or hexamers in solution,[9] it is useful to narrow our attention to the homodimeric form of the amine transaminase from *Luminiphilus syltensis* (LS_ATA) (**Figure 2,** last section). Each subunit has its own active site, but in each dimer pair the adjacent subunit complements the active site of the other. An informative review of the active organization in fold type IV transaminases has been written by Bezsudnova et al..[9]

The apoenzyme cannot catalyze the amine-transfer process without the assistance of the cofactor, pyridoxal 5'-phosphate (PLP). This Vitamin B_6 derivative, discussed in section 1.2, is coordinated in every subunit. In fold type IV enzymes, PLP fits in a cavity formed by amino acid residues in the C-terminal domain and is held in a specific orientation by non-covalent interactions. Polar amino acids, most commonly Arg and Thr create a hydrogen bonding network around the 5'-phosphate group of the cofactor and a Glu residue hydrogen bonds the pyridine nitrogen (**Figure 3**).[9] The arrangement of polar residues around the 5'-phosphate group is conserved among transaminases and is often referred to as the Pi "Binding Cup".[15,16] The capacity of transaminases to bind the cofactor has been linked to the operational stability of the enzyme,[17,18] because the apoenzyme is more susceptible to denaturation. When the holo enzyme is in its resting state, the aldehyde group of the PLP cofactor is covalently bound to the enzyme through an imine bond with the ε-amino group of a lysine. This covalently bound PLP with the Lys is known as internal aldimine (**Figure 3 and 4**). This complex exists in all PLP-depended enzymes, even in glucan phosphorylases where the carbonyl group of PLP does not participate in the reaction cycle (E.C. 2.4.1.1). Transaminases are usually crystalized in the internal aldimine conformation. During the transamination reaction this lysine residue plays an important role in the catalytic cycle and will from now on be referred to as the catalytic lysine. The aldimine covalent bond between PLP and the catalytic lysine is broken when the substrate enters the active site of transaminases and is regenerated in the final step of the reaction cycle (section 1.6).

A two-pocket substrate binding model was first deduced from a structure-reactivity study conducted by Shin and Kim for the fold type I ω-TA from *Vibrio fluvialis.*[19] This model fits to all enzymes that display transamination activity.[20] The two pockets differ in size. In (*R*)-selective amine transaminases ((*R*)-ATAs), the large binding pocket is located

above the 3'-pyridine oxygen of the PLP cofactor and the small binding pocket above the 5'-phosphate group (**Figure 3**). The large pocket is lined with both hydrophobic and polar amino acids and can thus coordinate both the phenyl group of the amine donor as well as the α-carboxylate group of the keto-acid amine acceptor. In other words, the same cavity can bind two chemically distinct species, a dual substrate recognition property of the large binding pocket that is commonly found in (*R*)-ATAs.[7] In (*S*)-ATAs, the dual substrate recognition is attributed to a highly conserved "flipping" Arg residue that orients its polar side chain towards the active site when the acidic amine acceptor is bound, but turns towards the solution when the amine donor enters the active site.[5]

Due to the relative positions of the binding pockets, when the incoming amine substrate condenses with the PLP, two of the amine donor substituents are in the same plain of the π molecular orbital system of the pyridine ring of PLP. The fourth bond of the tertiary carbon of the amine substrate (in the case of primary amines, the proton) is oriented perpendicular to the PLP plane.[21] This orientation of the C-H bond is important for the enzyme catalyzed reaction to proceed (section 1.6).

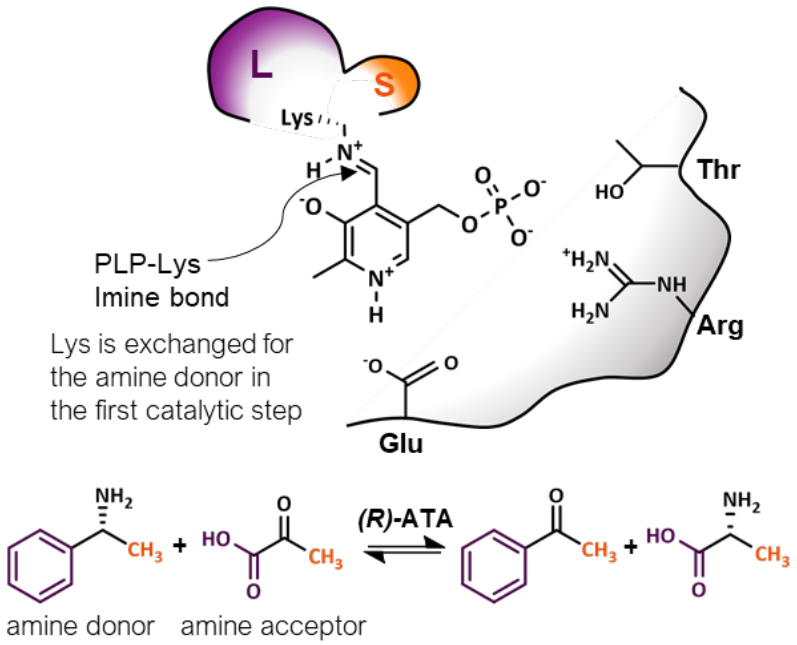

Figure 3. Schematic diagram of the large (L) and small (S) binding pockets in (*R*)-ATAs, and the functional groups of the side chains of common residues that coordinate the pyridine nitrogen and the 5'-phosphate moiety of the cofactor in fold type IV transaminases. The amine donor and the amine acceptor sequentially bind on the PLP cofactor during the reaction. The transamination reaction between (*R*)-1-phenylethylamine and pyruvate is shown in the bottom. The substituents of the reactants that fit in the L pocket are colored in purple, while the substituents that fit in the S pocket are colored in orange.

The large and the small binding pockets in (*R*)-ATAs occur in a cleft between the N- and the C-terminal domain of the first subunit close to the dimer interface (**Figure 4**).[9] The βX and βY strands of the N-terminal domain and the β-turn of the C-terminal domain of each subunit contain residues critical for substrate binding. The loop from the adjacent subunit also participates in the formation of the active site. It is common for multidomain proteins, to bind the substrates in cavities formed between the domains because this arrangement satisfies the need for a flexible interaction between the protein and the substrates.

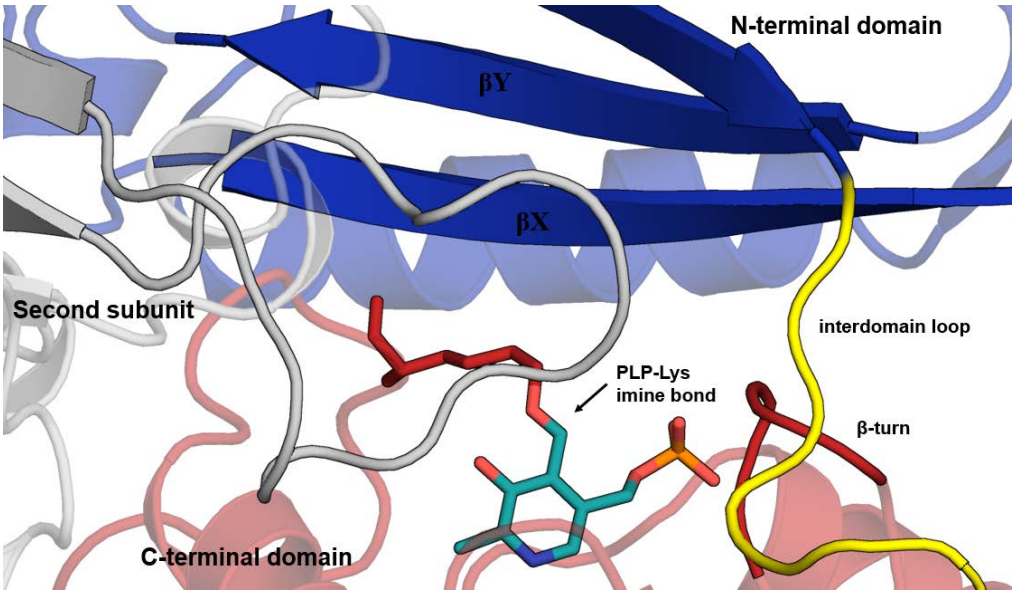

Figure 4. The active site of ATA from *Luminiphilus syltensis* (LS_ATA, PDB code 7p3t). The N- and C-terminal domains are colored blue and red respectively and the adjacent subunit is colored white. The PLP-lysine complex is shown in sticks (elemental coloring with cyan for C atoms of PLP while all atoms of the Lys residue are shown in red). The βX and βY strands of the N-terminal domain, the β-turn of the C-terminal domain, and the two loops are important secondary elements of the structure that define the interactions between the protein and the substrates.

1.5 Sequence-function relationships among fold type IV enzymes

Höhne et al.[22] proposed characteristic sequence motifs that discriminate between the different families of fold type IV enzymes. At the time the study was published, only one enzyme with transamination activity towards (*R*)-amines had been reported. Close examination of the large and small binding pockets in the structures of known L-branched-chain amino acid transaminases (BCATs), D-amino acid transaminases (DAATs) and 4-amino-4-deoxychorismate lyases (ADCLs) generated a pattern of important functional residues which was refined by multiple alignment of sequences

from the three families. Since only one available structure of an (*R*)-ATA existed, the group managed to rationally construct the pattern of amino acid side chains that would allow the coordination of primary amines in the active sites of BCATs and DAATs. The constructed motif managed to identify genes from the NCBI database that encoded proteins with the desired function; the study revealed twenty-one (*R*)-ATAs. The (*R*)-selective ATA from *Luminiphilus syltensis* (LS_ATA) used in this thesis, was among those twenty-one enzymes and was previously mentioned as *Gamma proteobacterium* ATA.[22]

The distribution pattern of functionally important amino acid residues for each of the enzyme families of fold type IV transaminases, is divided in two sequence motifs (motif 1 and 2). The LS_ATA does not share any of the sequence motifs identified for BCATs, DAATs, ADCLs or (*R*)-ATAs. Only the sequence of the β-turn (^{248}STAG^{251}) resembles the ^{273}TTAG^{276} (numbers correspond to the (*R*)-ATA from *Aspergillus fumigatus*, PDB code 4chi) motif commonly found in (*R*)-ATAs.[9]

1.6 Transamination mechanism

A model reaction mechanism was first described for the fold type I mitochondrial aspartate transaminase.[23] The mechanism of the transamination reaction between (*R*)-phenylethylamine ((*R*)-PEA) and pyruvate as substates will be described here in a simplified form. More detailed mechanisms have been proposed.[24,25]

The pyridoxal 5'-phosphate (PLP) cofactor is bound to the apoenzyme through non-covalent interactions, but also through an imine bond between the ε-amino group of the catalytic lysine and the aldehyde 4' carbon of PLP, as described in section 1.4. Since the imine bond arises from the condensation of the amine group with an aldehyde, the resulting imine is an aldimine. Later in the reaction cycle a ketimine species is formed which is the imine resulting from the reaction between an amine and a ketone. This structure of the PLP-Lys aldimine is depicted in **Figure 5A** and is known as an "internal" aldimine. When the amino donor, (*R*)-PEA, enters the active site, it acts as a nucleophile that attacks the iminium carbon of the internal aldimine. The lysine-PLP imine bond is broken and a substrate-PLP imine bond of the same sort is made forming a compound known as an "external" aldimine (**Figure 5B**). This process is termed transaldimination.

In the external aldimine the electrons of the C-H bond of the substrate are delocalized into the PLP ring. This is due to the fact that the sp^3 orbital of the tetrahedral carbon of the amino donor substrate that forms the σ bond with the hydrogen atom is parallel to

the π molecular orbital system of the PLP cofactor.[21,23] In the next step the catalytic lysine abstracts the proton from the tetrahedral carbon of the substrate. The conjugated system

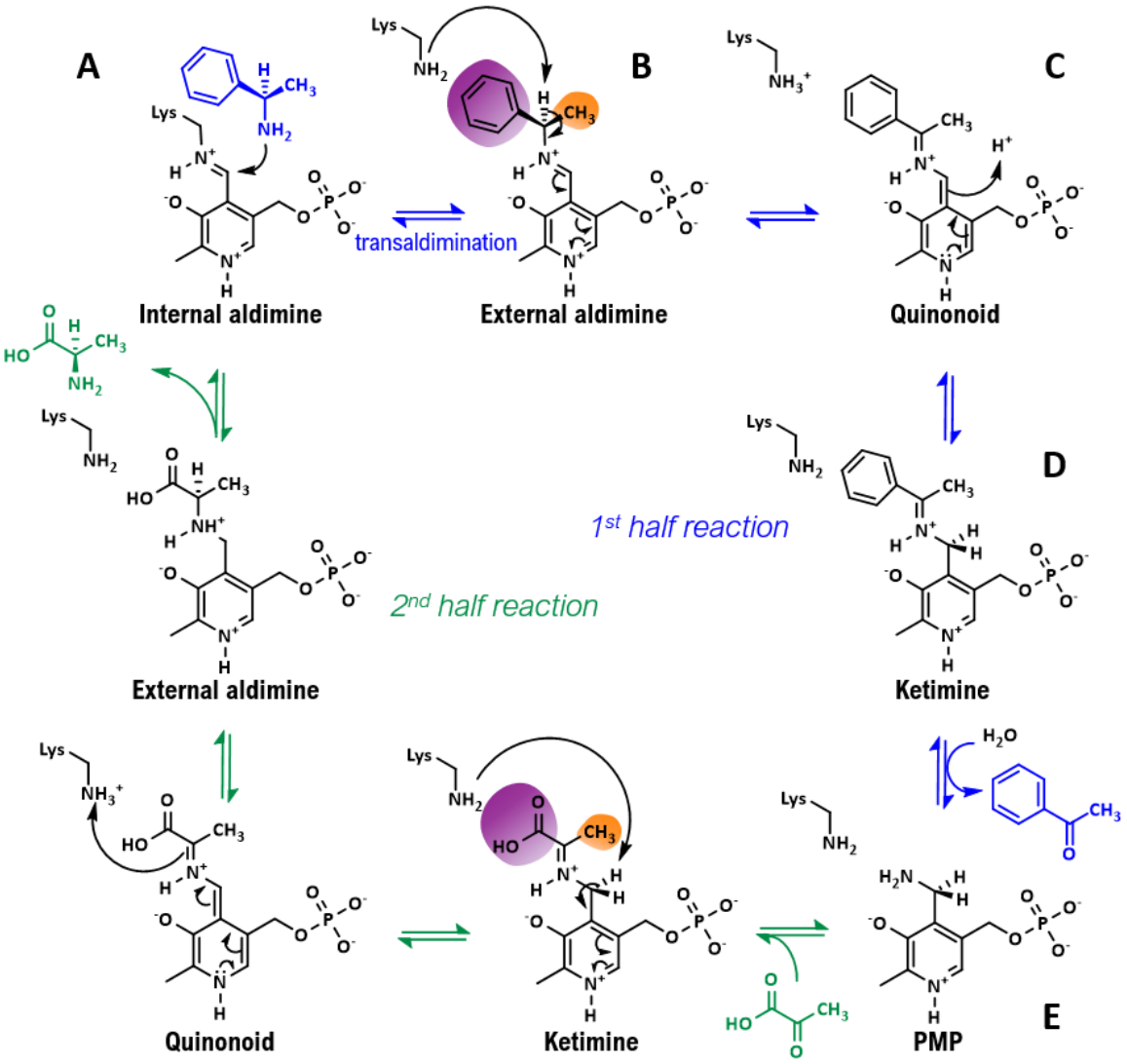

Figure 5. Reaction mechanism for the transamination reaction between (*R*)-PEA (amine donor) and pyruvate (amine acceptor). The exchange of the amino group between the two compounds occurs through a two-part reaction, with PLP being the intermediary. In the first half reaction, the aldehyde of PLP forms an imine bond with a lysine residue **(A)** and activates the iminium carbon for nucleophilic attack. The incoming (*R*)-PEA forms a new imine bond with the cofactor **(B)**. The protonated pyridine nitrogen acts as an electron sink that stabilizes the negative charge that evolves on the substrate after proton abstraction **(C)**. Compound **C** is reprotonated on the 4' carbon. In the ketimine compound **(D)** that is formed, the original imine bond formed in compound **A** has effectively moved to an adjacent position (respective bonds colored red). This new imine bond is then hydrolyzed to acetophenone and PMP. PMP can now transfer the amine group to pyruvate in the second part of the reaction to produce D-alanine. The substituents of the two substrates in the internal aldimines that occupy the large and the small binding pockets in the enzyme active site are highlighted in purple and orange, in correlation to Figure 3.

of PLP neutralizes the negative charge that would otherwise form on the carbon. The resulting compound (**Figure 5C**) is called a quinonoid intermediate, because it is similar to *p*-quinones. The formation of the quinonoid intermediate is regarded to be the most energy demanding among all reaction steps,[24,26] and thus determines the reaction rate. Reprotonation occurs on the 4' carbon of the cofactor and results in a ketimine intermediate (**Figure 5D**). Hydrolysis of the imine bond releases the first product of the reaction, acetophenone, and pyridoxamine 5'-phosphate (PMP) (**Figure 5E**). This is the first half of the reaction cycle.

In the second half-reaction, pyruvate, the amine acceptor, is converted to D-alanine following the same reaction steps in reverse. Pyruvate undergoes a nucleophilic attack by the amine group of PMP. A ketimine is formed which is converted to an external aldimine via the quinonoid intermediate. Transaldimination then leads to the internal aldimine and formation of the second product of the reaction, D-alanine. The end result of the second half-reaction is the reductive amination of the ketone. This however is achieved by amine transfer and not though reduction of the imine from a reducing agent such as $NaCNBH_3$, as an organic chemist would do. The benefit of the enzyme catalyzed transamination reaction is that in this way the reaction is enantioselective, as explained in detail in the next section (section 1.7).

1.7 Reaction stereoselectivity and what it takes to achieve it

Amine transaminases accept only a single enantiomer of the amine donor to form the corresponding prochiral ketone. Then, the enzyme accepts a different prochiral ketone and transforms it to a new amine. The configuration of both the amine donor and the amine that is produced is the same.

To see how the stereoselectivity of the reaction arises it is easier to look at the second half-reaction where the enzyme creates the chiral amine (in this case D-alanine) from a prochiral substate (pyruvate). If the substrate is prochiral and the product is generated in great enantiomeric excess, then there should exist an intermediate with heterotopic faces where the reaction takes its stereoselective path (**Figure 6**). Indeed, by placing the 4' prochiral trigonal carbon of the quinoid intermediate formed between pyruvate and pyridoxamine, in the center of the plane and counting down the groups in priority 1-3, two enantiotropic faces exist, depending on the position of the catalytic lysine. In (*R*)-ATAs, and in all PLP depended enzymes of fold type IV, the catalytic base is positioned to the *re* face of the plane. The catalytic lysine abstracts the pro-*R* proton from the 4' carbon of the ketimine. Then the proton is added on the iminium carbon of the substate

from the *re* face of the plane and only D-alanine can be formed. Since the process of breaking and making the two C-H bonds involves the same face of the plane, the hydrogen transfer is regarded a suprafacial transfer mediated by the catalytic base.

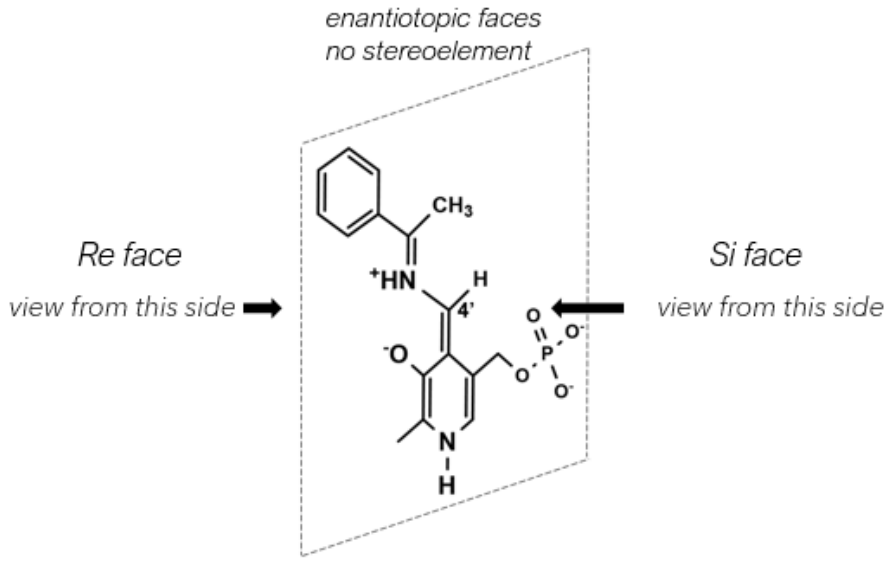

Figure 6. *Re*/*Si* faces can be assigned to the planar quinonoid intermediate of (*R*)-PEA, based on the stereochemistry of the 4' trigonal carbon of PLP.

The same principles apply to the first half of the reaction as well. The proton to be abstracted from the amine donor is perpendicular to the plane of the external aldimine to the *re* face and thus accessible to the catalytic lysine. Addition of a proton to the *re* face of the quinonoid intermediate leads to a ketimine with a pro-*R* proton. Thus, the topography of the active site is not only important for the acceptance of the "correct" enantiomer but also for the transamination reaction itself to occur. The active site of amine transaminases with (*S*)-enantioselectivity (fold type I), mirrors the active site of (*R*)-selective transaminases in the sense that the catalytic lysine is located in the "back" of the cofactor (the *si* face of the cofactor plane).[27]

1.8 Routes to optically pure amines with amine transaminases

From the discussion in section 1.7, it becomes apparent that the selectivity of the enzyme is governed from the interactions developed between the substrates and the residues in the small and large binding pocket, as well as the positioning of the catalytic lysine in the *re* or *si* enantiotopic face of the cofactor's pyridine plane. When an (*R*)-selective amine transaminase such as the amine transaminase from *Luminiphilus syltensis* (LS_ATA) is exposed to a racemic mixture of (*R*,*S*)-PEA in the presence of

pyruvate, the (*R*)-enantiomer undergoes catalysis in a higher rate. If the enzyme has very high enantioselectivity, the (*R*)-enantiomer is converted to acetophenone (50% conversion) and the (*S*)-enantiomer remains as is. At the same time, pyruvate accepts the amine group of (*R*)-PEA and is transformed to D-alanine. This process is known as kinetic resolution of the phenylethylamine racemate (**Figure 7**). The difference between kinetic and classical resolution is that in classical resolution both enantiomers react completely with a chiral reagent forming diastereomeric derivatives, which can then be separated.

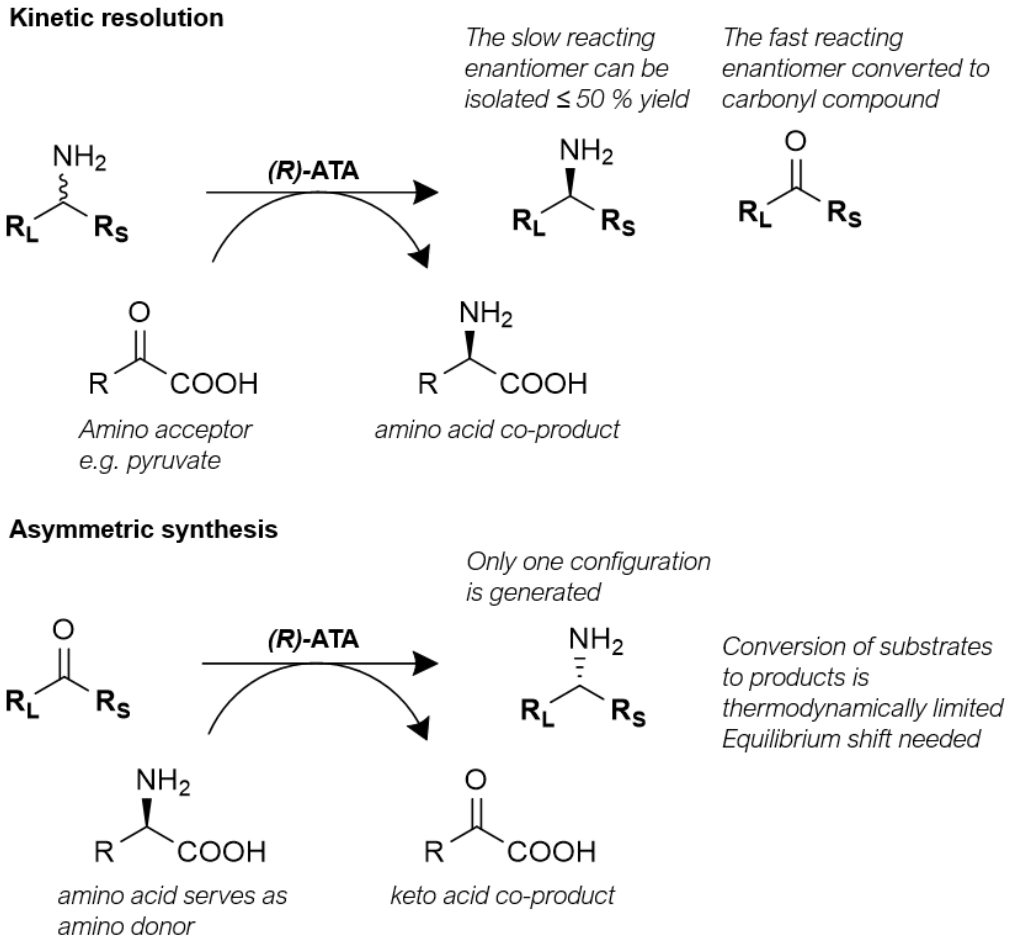

Figure 7. Strategies for preparing optically active primary amines using amine transaminases (ATAs). Both strategies have been adopted in order to produce primary amines in optically pure form. Kinetic resolution separates the product (the slow reacting enantiomer) from the starting racemic material. Asymmetric synthesis can produce high yields of enantiomerically pure primary amines but it is practically more tedious because of the unfavorable thermodynamic equilibrium.

While kinetic resolution destructs the chirality (in this case) of the (*R*)-enantiomer in order to isolate the other, asymmetric synthesis refers to reactions that selectively create

only one of the two possible configurations of a prochiral substrate (**Figure 7**). If the target is to synthesize (*R*)-PEA by employing an (*R*)-ATA, then acetophenone (prochiral unit) and alanine (amino donor) must be used as substrates. The amine transaminase will act only on the *re* face of the trigonal carbon of the ketimine intermediate of acetophenone and yield only the (*R*)-enantiomer of 1-PEA. In other words, the reaction depicted in **Figure 5** should run in reverse. However, the fact that a mechanism for the deamination of alanine and the conversion of acetophenone to phenylethylamine exists it does not mean that the reaction proceeds. In fact, the asymmetric synthesis of many optically pure primary amines is thermodynamically hindered.[28,29]

The achievable conversion of substrates to products in any of the two possible reaction routes of **Figure 8** is governed by the position of the chemical equilibrium. Addition of the enzyme to a solution of pure acetophenone and alanine or to a different solution of pure phenylethylamine and pyruvate will drive the reaction to the same equilibrium point where a mixture of all four compounds exists. However, the concentrations of acetophenone and alanine at equilibrium will always be higher than the concentrations of phenylethylamine and pyruvate. Alternatively stated, the reaction, in the direction written in **Figure 8**, which would lead in the asymmetric synthesis of optically pure 1-phenylethylamine, "lies to the left". Equilibrium is reached when only a small amount of the reactants (i.e., acetophenone and alanine) has been converted to products (i.e., 1-phenylethylamine and pyruvate). The position of the equilibrium for any reaction can be deduced from the value of the equilibrium constant K_{eq}. The equilibrium constant (K_{eq}) for the aforementioned reaction is expressed as:

$$K_{eq} = \frac{[PEA][pyruvate]}{[acetophenone][alanine]}$$

The value of K_{eq} has been experimentally determined (8.8×10^{-4}).[29] When the K_{eq} value is lower that than 10^{-3}, then the equilibrium lies on the side of the substrates. Reactions with $K_{eq} > 10^{-3}$ are considered to favor the products, and intermediate values of K_{eq} favor neither the reactants not the products.

Because chemical equilibria are dynamic, the composition of the reaction at equilibrium responds to changes in the reaction conditions. Many groups have utilized Le Chatelier's principle in order to shift the equilibrium towards the synthesis of 1-phenylethylamine.[30] These studies include large excess of the amine donor in the reaction mixture,[28,30] removal of one or both of the products as they are formed through enzymatic[28,31,32] or physical means[33], or spontaneous chemical transformation of the co-product to unreactive species.[34,35,36]

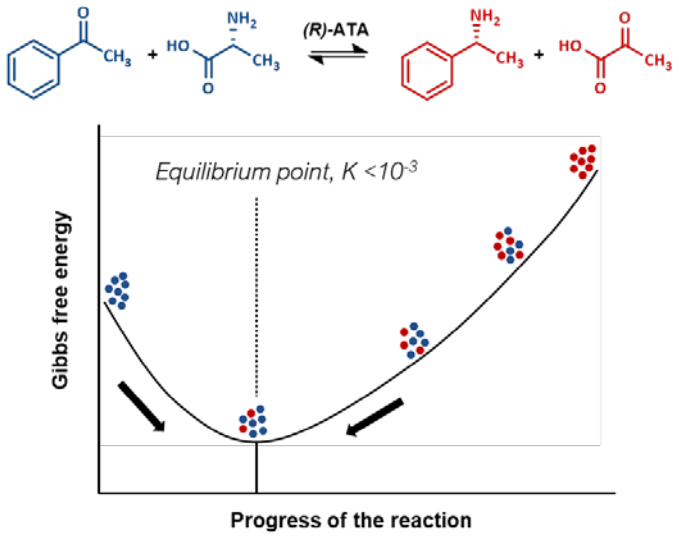

Figure 8. At the top the transamination reaction is depicted in the direction of the asymmetric synthesis of 1-phenylethylamine and pyruvate (here regarded as products, red) from acetophenone and alanine (substrates, blue). The Gibbs free energy (G) of a reaction is plotted as a function of the composition of the reaction mixture starting from pure substrates (blue dots on the left side) to pure products (red dots on the right side). What is important is not the function itself but the slope of the function, the derivative of G with respect to the different reactant/product concentrations as the reaction proceeds (i.e., ΔG). The point where the slope equals to zero (ΔG= 0), lies close to the reactants and thus 1-phenylethylamine formation is thermodynamically limited. This diagram was best described in an analogy by Isaac Asimov.[37] The curve is like a V shaped double incline with the reactants (i.e., acetophenone and alanine) and the products (i.e., phenylethylamine and pyruvate) sliding down as bricks from the top edges. The enzyme enhances the rate of their slide by acting as a coating that reduces the friction between the surface and the bricks. Looking at the diagram from above creates the misconception that the enzyme halts the reaction at a random position. If the view is from the side, it becomes apparent that the reaction is pulled to only one direction: downwards to the Gibbs free energy minimum of the system.

Because chemical equilibria are dynamic, the composition of the reaction at equilibrium responds to changes in the reaction conditions. Many groups have utilized Le Chatelier's principle in order to shift the equilibrium towards the synthesis of 1-phenylethylamine.[30] These studies include large excess of the amine donor in the reaction mixture,[28,30] removal of one or both of the products as they are formed through enzymatic[28,31,32] or physical means[33], or spontaneous chemical transformation of the co-product to unreactive species.[34,35,36]

1.9 Objectives of the thesis

A common limiting factor for the exploitation of transaminases for industrial purposes are the steric constrains imposed by the small binding site which limit the capacity of the enzyme to facilitate the biotransformation of many amine substrates. Our protein engineering efforts aimed to construct a variant that would overcome the wild-type's substrate limitations and that could be used to prepare enantiomerically enriched forms of the compounds shown in **Figure 9**. Rational design requires knowledge of the architecture of the active site upon substrate binding of the target compounds. The high resolution structure of the amine transaminase in the internal aldimine state, resolved in collaboration with the group of Prof. Tsiotis and their partners,[14] was a reliable starting template. Because the C-N bond that is broken/made, is the imine linkage to the cofactor, the transamination reaction has a complex mechanism with more reaction intermediate steps than the other reactions catalyzed by PLP-depended enzymes. Simulating the quinonoid intermediate of the target phenylamines in the active site, would allow us to study the amino acid residues that are in direct contact with the alkyl chain of each substrate. The quinonoid compound is the most energy demanding intermediate among the reaction steps, thus engineering an active site that effectively stabilizes the quinonoids of interest is more likely to produce active variants.

Many mutagenesis studies have showed that the exclusion of bulky substituted substrates corelates with a higher number of van der Waals unfavorable overlaps in the small binding pocket in both (*S*)- and (*R*)-selective ATAs.[38,39,40] Rational design studies have used alanine scanning mutagenesis in order to excavate the small binding site and permit the entry of bulkier substates.[15,41] The term "excavating" is quite literal, because the side chains of amino acid residues that are thought to block the coordination of bulkier substrate substituents are truncated, by mutating them to a smaller amino acid, such as alanine. Although glycine is the smallest residue, with no substituent as side chain, it is also the only amino acid that lacks a Cβ. Replacing any residue with glycine would allow for more conformational flexibility than the parental one, and this could lead to structural changes. The opposite strategy, of making the active site shallower by introducing residues with bulky and rigid side chains is used in rational design studies aiming to improve the stereoselectivity of the enzyme.[42] Improving the substrate scope of the amine transaminase without compromising the enzyme's enantioselectivity is one of the objectives of this study.

Our second and final objective was to find the right combination of reaction conditions and literature methods that would allow the enzyme variants to act as an effective asymmetric catalyst of optically pure primary amines.

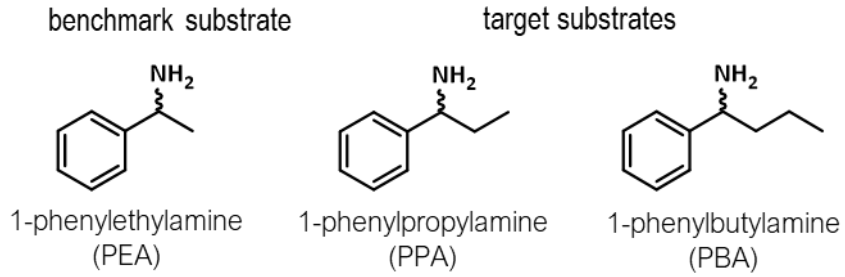

Figure 9. Arylalkylamines used in this study.

CHAPTER 2

Materials and Methods

2.1 Chemicals

The arylalkylamines and their respective ketones needed for biotransformation experiments, 1-phenylethylamine racemate (98%), (*R*)- and (*S*)-1-phenylethylamine (98%), (*R*)- and (*S*)-1-phenylpropylamine (99+%), (*R*)-1-phenylbutylamine (98%), and acetophenone (99%) were purchased from Alfa Aesar while 1-phenylpropylamine racemate (97%), propiophenone (99%) and butyrophenone (99%) from Sigma Aldrich. The organic solvents, ethanol (≥98%), dimethyl sulfoxide (99.9%) and ethyl acetate (≥98%) were purchased from Honeywell, Scharlau and Fisher Chemical respectively. All other reagents are of analytical grade and were purchased from the following manufacturers, listed in alphabetical order: AcumediaLAB, Alfa Aesar, Carl Roth, Fluka, LabChem, Merck, Nippon Genetics, Serva, Scharlau and Sigma-Aldrich. Glucose dehydrogenase from *pseudomonas sp*. (>200 U mg^{-1}, GDH) and L-lactic dehydrogenase from rabbit muscle (600 U mg^{-1}, LDH) were both suppled from Sigma-Aldrich. DpnI (1000 U) was purchased from NEB along with the 1 kb Plus DNA Ladder, SDS-PAGE blue loading buffer 3x and the agarose gel loading dye.

2.2 Recipes for buffers, solutions and separation gels

All the buffers, solutions and separation gels needed for the methodologies described in Chapter 2 are presented in Table 1.

Table 1. Recipes for buffers and solutions and separation gels.

Experiment	Buffer/solution	Components
Cell culture	LB medium	1% Tryptone, 0.5% Yeast Extract, 1% NaCl 1.5% Agar was added for solid cultures
	LB SOC	1% Tryptone, 0.5% Yeast Extract, 1% NaCl, 2.5 mM KCl, 10 mM Magnesium chloride ($MgCl_2$), 10 mM Magnesium sulfate ($MgSO_4$),20 mM Glucose
Chemo-competent cells	RF1	100 mM Rubidium chloride (RbCl), 50 mM Manganese chloride ($MnCl_2$), 30 mM Potassium acetate (CH_3CO_2K), 10 mM Calcium chloride ($CaCl_2$), 15% ($^{v}/_{v}$) Glycerol Buffer calibrated to pH 5.8 using Acetic acid
Chemo-competent cells	RF2	10 mM Rubidium chloride (RbCl), 10 mM 3-morpholinopropane-1-sulfonic acid (MOPS), 75 mM Calcium chloride ($CaCl_2$), 15% ($^{v}/_{v}$) Glycerol Buffer calibrated to pH 7.0 using NaOH
SDS-PAGE electrophoresis	Resolving gel buffer	1.5 M Tris-HCl pH 8.8, 0.4% ($^{w}/_{v}$) SDS
	Stacking gel buffer	0.5 M Tris-HCl pH 6.8, 0.4% ($^{w}/_{v}$) SDS
	Running Buffer 10x	250 mM Tris, 1.9 M Glycine, 1% ($^{w}/_{v}$) SDS
Agarose electrophoresis	TAE buffer 50x	2 M Tris, 1 M acetic acid, 0.5 M EDTA, pH 8.0
Protein purification	Lysis Buffer	50 mM KPi, 300 mM NaCl, 0.1 mM PLP, 15 mM Imidazole
	Wash buffer	50 mM KPi, 300 mM NaCl, 0.1 mM PLP, 30 mM Imidazole
	Elution buffer	50 mM KPi, 300 mM NaCl, 0.1 mM PLP, 300 mM Imidazole

Separation method		Components	
SDS-PAGE electrophoresis	Resolving gel 12.5%	H_2O	5,33 mL
		Acrylamide/bis mix 30%	6,67 mL
		Resolving gel buffer	4 mL
		Ammonium persulfate (APS) 10%	80 µL
		Tetramethylethylenediamine (TEMED)	8 µL
	Stacking gel 4%	H_2O	4,95 mL
		Acrylamide/bis mix 30%	1,07 mL
		Stacking gel buffer	2 mL
		Ammonium persulfate (APS) 10%	80 µL
		Tetramethylethylenediamine (TEMED)	8 µL
Agarose gel electrophoresis		Agarose	0.56 g
		TAE buffer 1x	70 mL
		Ethidium bromide	1 µL

2.3 Bioinformatic analysis

2.3.1 Structure refinement and energy minimization

The hexameric crystallographic structure (PDB code 7p3t) was refined by molecular dynamics simulation (md_refine.mcr) using the YAMBER3 force field in YASARA Structure suite v. 20.10.4 (http://www.yasara.org). The parameters that were applied were the following: 25^{o}C, pH 7.4, 500 ps, collect one snapshot every 25 ps. The conformation with the lowest potential energy was chosen for further studies. The stereochemical validity of the structure was checked using the MolProbity platform.[43]

The quinonoid intermediate structures of the target substrates were built manually on the pyridoxal 5'-phosphate (PLP) cofactor of the best active site of the refined structure, as indicated from the MolProbity analysis. In order to improve the geometries in the active site, the model was energy minimized. First, a local energy minimization was performed, allowing only the atoms of the substrate to move and position in the active site. Then, in a second round of energy minimization, the polypeptide chains and the quinonoid molecule were allowed to move except for the PLP pyridine nitrogen which anchors the cofactor to the apoenzyme though a hydrogen bond. Finally, we performed a global energy minimization allowing every atom in the structure to move. All molecular graphics were prepared using PyMOL v.0.99 (http://www.pymol.org).

2.3.2 Calculation of formation energy of (*R*)- and (*S*)-PEA quinonoids

Energy calculations were conducted using YASARA Structure suite v. 20.10.4 (http://www.yasara.org). All water molecules were first removed from the structure using the command 'DelWaterObj' that deletes all atoms that belong to water molecules including OH^-, H_3O^+ and single oxygen species. Before performing the energy calculation, the structure was optimized as follows:

Edit < Optimize < Molecule and the quinonoid intermediate of (*R*)- or (*S*)-phenylethylamine was chosen.

Then the "Semi empirical Quantum mechanics (MOPAC)" was selected from the optimization methods window.

The energy (heat released or absorbed at constant pressure) during the formation of each quinonoid intermediate in the active site of the enzyme was calculated by selecting Analyze < Energy < Formation energy < Molecule.

2.3.3 Display of atom classes in the active site

The nonbonded overlaps of the van der Waals radii (bumps) between the atoms of the substrates and the amino acid residues in the active site were displayed in PyMOL (v.0.99, http://www.pymol.org) using the show_bumps.py script (Author: Thomas Holder) which is available to download from the PyMOL Wiki. In order to install the plugin, we selected Plugin > Install New Plugin > Choose File and selected the show_bumps.py.

Once the plugin was installed, a selection of the atoms of interest was created and bumps were displayed by using the command 'show_bumps [selection [, name]]'.

The following parameters were applied:

set sculpt_vdw_vis_min, 0.2

set sculpt_vdw_vis_mid, 0.3

set sculpt_vdw_vis_max, 0.4

show_bumps [selection]

2.4 Preparation and transformation of chemocompetent *E. coli* cells

A small-scale liquid culture of the respective strain of *E. coli* in LB media was grown overnight at 30°C, 220 rpm. One mL of the preculture was inoculated in 100 mL of LB medium and grown at 37°C to an OD_{600} (optical density at 600 nm) of 0.3 to 0.5 (approximately 2.5 h). The culture was left on ice for 15 min and then centrifuged for 20 min, 3.000 x *g*, 4°C. The supernatant was poured off and the pellet was resuspended in 20 mL of RF1 buffer. The resuspensions were left on ice for 15 min and centrifuged again for 20 min, 3.000 x *g*, 4°C. After discarding the supernatant, the cells were resuspended in 4 mL of RF2-buffer, left on ice for 15 min and aliquoted (50 µL) in polypropylene tubes. The aliquoted cells were frozen immediately at -80°C using liquid nitrogen.

To transform the chemocompetent cells, 2 µL of isolated plasmid DNA or DpnI digested DNA from PCR reactions was dispensed in a 50 µL aliquot of competent cells and placed on ice for 30 min. The cells were heat shocked by placing the tube for 30 sec in the thermoshaker (CellMedia) at 42 °C and then left on ice for 2 min. One mL of LB SOC

was added in the tube which was then incubated at 37°C for 1 h, 170 rpm. Aliquots of the transformation culture were plated on LB agar with ampicillin (100 μg mL^{-1}).

2.5 Mutagenesis

The pGaston vector containing the gene of the wild-type amine transaminase from *Luminiphilus syltensis* (LS_ATA) with a C-terminal 6xhis-tag sequence (3.371 bp) was used as the plasmid DNA template for the mutagenesis experiments. The master mix used to perform PCR reactions contained 0.25 μL of a high-fidelity DNA polymerase provided by Minotech biotechnology (IMBB-FORTH), with 5 μL of its 5x HF polymerase buffer (containing 7.5 mM $MgCl_2$), 0.2 mM dNTPs, 0.5 μM of each primer (**Table 2**), 0.2 ng/μL template plasmid, in 25 μL final volume. The buffers, the primers and the plasmid were pipetted together, while the dNTPs and the plasmid were added just before the reaction was initiated.

Table 2. The forward (fw) and the reverse (rv) primers used for the construction of the variants. The OligoCalc platform[44] was used to check each sequence for self-complementarity and to calculate the melting temperature (Tm) and %GC content.

Target mutation	Primer sequence	Tm (salt adjusted), °C	GC content, %
V37 fw	GTT TTT GAT GCT GTT AGC GCC TGG	62.4	50
V37 rv	GGC GCT AAC AGC ATC AAA AAC ACC	62.5	50
S248A/T249A fw	GTT TAC CTG TGC CGC CGC AGG C	69.5	68
S248A/T249A rv	GCG GCG GCA CAG GTA AAC ACT TC	68.3	61
S248A fw	GTT TAC CTG TGC CAC CGC AGG C	67.9	64
S248A rv	CGG TGG CAC AGG TAA ACA CTT CAT C	67.4	52
T249A fw	GTT CTG CCG CAG GCG GTG	62.9	72
T249A rv	GCG GCA GAA CAG GTA AAC ACT TC	64.6	52

The PCR was carried out under the following conditions:

Initial denaturation	98°C	30 s	
Denaturation	98°C	10 s	
Annealing	65°C or 70°C	30 s	25 cycles
Elongation	72°C	1 min 45 s	
Final extension	72°C	3 min 30 s	

The amplified product was detected by agarose gel electrophoresis using 0.8% ($^{w}/_{w}$) agarose and 1 kb DNA Ladder (NEB) as standard. The parental plasmid was digested by DpnI (NEB) for 1 h at 37°C. The samples were heated at 80^{o}C for 10 min to inactivate the restriction enzyme. After treatment with DpnI, PCR products were transformed into chemically competent *E. coli* TOP10 cells. Transformed cells ere plated onto LB agar plates supplied with ampicillin (100 µg mL^{-1}). Monoclonal colonies were picked and incubated in 5 mL LB cultures. The NucleoSpin Plasmid Kit (Macherey-Nagel) was used for plasmid isolation. The concentration of the purified plasmid was determined photometrically at 260 nm using a µDrop™ Plate on the Multiskan Sky Microplate Spectrophotometer (Thermo Scientific). The correct sequences of the constructs were confirmed by Sanger sequencing (Genewiz, DE). The mutated plasmids were transformed into chemo-competent *E. coli* BL21 (DE3) cells for expression.

2.6 Recombinant protein expression and purification

The genes of interest were heterologously expressed in BL21(DE3) *E. coli* cells. Cells either from glycerol stocks or from single colonies were grown at small volume LB pre-culture overnight, at 30^{o}C, 220 rpm. The freshly grown pre-culture was suspended in 500 mL liquid LB media supplied with ampicillin (100 µg mL^{-1}) and grown at 37^{o}C, 120 rpm. The expression of the recombinant protein was induced with 0.2% ($^{w}/_{v}$) Rhamnose when the OD_{600} of the culture reached 0.6-0.8 (typically 3-4 h after inoculation). A small sample (volume equal to 10/OD_{600}) was taken from the culture before induction, pelleted by centrifugation at 10 000 rpm for 8 min, and stored at -20^{o}C, to be used in SDS-PAGE. The induced culture was incubated at 20^{o}C, 350 rpm for 16 to 18 h. A second 10/OD_{600} sample was removed from the culture and treated as before in order to be used in SDS-PAGE experiment. The rest of the culture was harvested by centrifugation (5 000 rpm, 30 min) and stored at -20^{o}C. For SDS-PAGE, samples were denatured in SDS-PAGE Sample buffer 3x, heated for 10 min, 95^{o}C, separated on 12,5% hand cast acrylamide gels and stained with Coomassie solution.

For purification, pelleted cells were resuspended in Lysis buffer and lysed by sonication (Amplitude 30%, Cycle 50%) for 5 min in total with intervals of 30 s. The sample was centrifuged for 10 min at 10 000 rpm and the crude lysate extract was filtered through 0.44 µm and 0.22 µm filters (Millipore). The sample was then loaded on a Ni-NTA 5 mL Protino® column pre-equilibrated with lysis buffer on the ÄKTA™ start FPLC system. Sample loading was performed with a 1.5 mL min^{-1} flow rate. The column was washed with 4 column volumes of Wash buffer, 3 mL min^{-1} flow rate). His-tagged recombinant

proteins were eluted with 3 column volumes of Elution buffer, 3 mL min^{-1} flow rate). The fractions containing the eluted recombinant protein were pooled and concentrated to a 2 mL final volume using centrifugal filters (30 kDa molecular weight cut-off, Amicon). The concentrated sample was desalted on a HiTrap™ 15 mL column equilibrated with phosphate buffer (50 mM, pH 7.5) containing 0.1 mM PLP. The purified enzyme solutions were aliquoted, flash freezed and stored at -20°C. The protein concentration was determined using the Bradford assay.

2.7 Photometric determination of enzyme activity

The activities of the enzyme preparations were determined by measuring the rate of product formation during the transamination reaction between 1-phenylethylamine and pyruvate, which leads to acetophenone and alanine.[45] Since the transamination reaction is inherently a two substrate and two product reaction the assay measures the rate dependence on the transformation between phenylethylamine and acetophenone while the second substrate, pyruvate, is supplied in excess. The acetophenone formed has a distinct absorption at 245 nm, due to the delocalization of electrons over the conjugated system of the carbonyl group and the phenolic ring. Other ketones with the same conjugated system such as propiophenone and butyrophenone show similar absorbance maxima. The extinction coefficient was determined to be 14.7 M^{-1} cm^{-1} for acetophenone and 10.18 M^{-1} cm^{-1} for propiophenone and butyrophenone, under the reaction conditions.

The reaction mixtures contained 1 mM enantiopure 1.0 mM (*R*)-amine donor, 2 mM sodium pyruvate, and 0.05 mM pyridoxal 5′-phosphate (PLP) in 50 mM HEPES buffer with 5 %(v/v) DMSO. Measurements were carried out in UV Star 96-well plates (Greiner) by adding 5 µL of the enzyme preparation, 10 µL of the amine donor solution (from a 20 mM stock solution in DMSO), 85 µL of the buffer and 100 µL of the sodium pyruvate solution (from a 4 mM stock solution in buffer). Sodium pyruvate was always added last, to initiate the reaction. All solutions used, except for the enzyme, where brought to room temperature before the assay. All measurements were performed in a Multiskan Sky Microplate Spectrophotometer (Thermo Scientific) in triplicates. The time-course of acetophenone formation at 245 nm was monitored for 5 min when less than 10% of the substrate is converted to product, so that the initial activity is monitored. Thus, standard curves of acetophenone and butyrophenone were defined between 0-0.08 mM (**Figure 10**).

By calculating the slope of the curve, the initial rate of the reaction can be obtained (ΔAbs/min). To express the rate in terms of the amount of product that is formed per unit time instead of absorbance change, ΔAbs/min is divided by the slope of the calibration curve (ΔAbs/mM). The rate is now expressed in μmol product formed per mL solution per min. The enzyme is added from a concentrated solution and therefore the actual enzyme concertation in the assay mixture should be taken into account (if 5 μL of a 5-fold diluted enzyme solution is used in a 200 μL assay mixture then the rate should be multiplied by a factor of 200). In order to get the expression of specific activity, the rate is divided by the mg of enzymes per mL (enzyme concertation determined by the Bradford assay) to calculate the specific activity of the enzyme (U mg^{-1}).

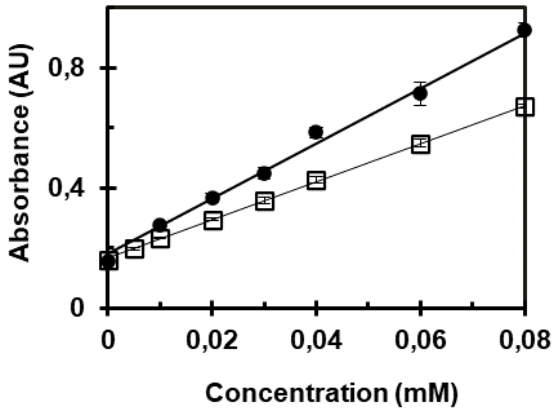

Figure 10. Standard curves of acetophenone (circles, R^2= 0.996) and butyrophenone (squares, R^2= 0.999).

2.8 Optimum pH and pH-stability

The enzyme (100 μL) was incubated without the substrates at three different 50 mM buffer solutions, KPi (pH 8.0), CHES (pH 9.0) and CHES (pH 10.0) supplemented with 0.1 mM PLP at 1.8 mL final volume. Buffer (85 μL) was added for each enzyme (5 μL), in order to have an enzyme/buffer ratio that is equal to that used in the activity assay. At different time points (0, 30 min, 1 h etc.), the 90 μL of each enzyme-mix was transferred to a 96-well plate. The initial activities were measured as in the activity assay by adding 10 μL of (*R*)-PEA (from a 20 mM stock solution in DMSO), and 100 μL of sodium pyruvate (from a 4 mM stock solution). Sodium pyruvate was diluted in ddH_2O so that the initial rates were measured in the same pH as the pH where the enzyme was incubated. The final buffer concentration during the reaction is 25 mM containing 0.05 PLP. The pH of the buffers was adjusted at 25°C, at the same temperature that the

incubation of the enzyme and the activity measurements took place. All measurements were performed in a Thermo Multiskan Sky Microplate Spectrophotometer (Thermo Scientific) in triplicates. Specific activities were calculated as described in section 2.7.

2.9 Pyridoxamine phosphate determination assay

The assay was performed according to Voss et al..[46] The half-transamination reaction was performed in 96-well plates with 50 μL of purified enzyme, in 200 μL final volume, in CHES buffer 50 mM pH 9.0. The amine donor (*R*)-PEA in 1.25% ($^{v}/_{v}$) ethanol was added last (2.5 mM final concertation), to induce PMP formation, while ethanol was used also in the samples without the amine, to observe the enzymes in the internal aldimine state. The change of absorbance from 290 to 470 nm was measured in a Multiskan Sky Microplate Spectrophotometer (Thermo Scientific) in triplicates.

2.10 Biotransformations

2.10.1 Kinetic resolution

Reactions were performed in a 2 mL scale in 2 mL polypropylene tubes containing 60 μg of purified amine transaminase. All amine substrates were dissolved in DMSO and then added in the reaction buffer with a 5% ($^{v}/_{v}$) DMSO final concentration. For the kinetic resolution of (*R,S*)-phenylethylamine and (*R,S*)-phenylpropylamine (97% pure Sigma Aldrich), 8 mM of the racemic amine donor was used and 16 mM of sodium pyruvate. (*R,S*)-phenylbutylamine was not commercially available so the single (*R*)-enantiomer was used as a substrate in kinetic resolution mode in 4 mM final concentration with 8 mM pyruvate. CHES buffer 50 mM, pH 9.0 supplied with 0.1 mM PLP was used for all reactions. The tubes were placed in a thermoshaker (CellMedia) at 35^{o}C, 750 rpm. The extraction method used to monitor the reactions and the gas chromatography (GC) analysis is described in section 2.10.3.

2.10.2 Asymmetric synthesis

Reactions were performed in 0.5 mL scale in 1.5 mL glass vials containing 70 μg up to 0,6 mg of purified enzyme in CHES buffer pH 9.0, 0.1 mM PLP, 35^{o}C, 600 rpm and were monitored after two and five days. For reactions utilizing the LDH/GDH enzymatic cascade higher enzyme concentrations (up to 0.6 mg) were used and they took place in

1 mL scale, in HEPES buffer pH 8.0, 0.1 mM PLP, 30^{o}C, 600 rpm. pH of 8.0 was used in this case to preserve the activity of LDH for the duration of the reaction. The extraction procedure and gas chromatography (GC) analysis described in section 2.10.3 was used for all reactions.

Reactions with IPA paired with acetophenone, propiophenone and butyrophenone contained 100 to 750 mM of IPA and 8 mM of the ketone. The amine donor, *p*-xylylenediamine was used in a final concentration of 24 mM and (*R*)-1-phenylethylamine in a final concentration of 8.8 mM with the same ketone concentration (8 mM) in both reactions. The amine donor D-alanine was used in racemic form (200 mM) supplied with D-glucose (200 mM), NADH (2 mM), 15 U mL^{-1} glucose dehydrogenase (GDH), 50 U mL^{-1} lactate dehydrogenase and 8 mM of the ketone.

2.10.3 Analysis via gas chromatography

In order to monitor the course of the reactions 200 µL samples were removed from the reaction at specific time intervals. Samples were quenched with 15 µL of 5 M NaOH. The pH becomes strongly alkaline (pH >12, checked with pH indicator papers) which deprotonates the amine species. The deprotonated amine and ketone substrate/products in the sample were then extracted by adding ethyl acetate (2x 200 µL) and using a vortex mixer. The two phases were separated by spinning down the mixtures. The organic phase was transferred in a clean tube and dried with anhydrous Na_2SO_4. The drying agent is pelleted at the bottom by spinning down the tube and the organic phase is transferred to a glass vial containing an 400 µL insert (Agilent). The conversion was determined by gas chromatography using Shimadzu Nexis GC-2030 system equipped with the chiral column Cyclodex-B (30 m x 0.25 mm x 0.25 µm) from Agilent. As a carrier gas we used He with 1.4 mL min^{-1} column flow. The detection was made with an FID which was set at 250^{o}C. The following program was used: 80°C initial temperature, heated to 120°C with 2°C min^{-1} and then to 220°C with 20°C min^{-1} where it is held for 3 min. Retention times: 13.8 min for (*R*)-PEA, 14.0 min for (*S*)-PEA, 15.4 min for acetophenone, 18.7 min for (*R*)-PPA, 18.9 min for (*S*)-PPA, 20.8 min for propiophenone, 23.5 min for (*R*)-PBA and 24.6 min for butyrophenone. A response factor for each compound was determined using standard solutions and was used for calculation of the conversion. The degree of enantiopurity was calculated based on enantiomeric excess of the starting substrates (ee_s) in equation:

$$ee_s = \frac{[S] - [R]}{[S] + [R]}$$

[S]: concentration of the (*S*)-enantiomer

[R]: concentration of the (*R*)-enantiomer

CHAPTER 3

Results and Discussion

3.1 Validation of the structural fold in the CATH database

The CATH[47] protein secondary structure database (version 4.1, http://www.cathdb.info) applies a threading method to obtain the optimal alignment of the target sequence against a library of known folds. It is even more accurate to upload the structure file (.pdb), instead of the sequence, of the target protein and find matching domains in the fold library. The algorithm accurately identified the fold of the N- and the C-terminal domain of the LS_ATA and also deduced that the protein with the best structural similarity for both domains was the branched-chain amino acid transaminase (BCAT) from *Geoglobus acetivorans,* (PDB code 5cm0). A manual search of similar sequences with the target sequence in protein data bank (PDB), leads to the same match. The two proteins have only a 40% sequence identity. This shows that the sequence space that LS_ATA lies is unexplored and thus LS_ATA''s structure elucidation, as well as its evolution, are of interest. Despite the results of CATH, no functional similarity is observed between LS_ATA and BCATs, since Hohne et al. has reported that the LS_ATA does not convert 3-Methyl-2-oxobutyric acid to valine.[22]

3.2 In silico modeling of the quinonoid intermediates

The group of Prof. Tsiotis and their collaborators provided us with a 1.6 Å structure of the wild-type (*R*)-selective amine transaminase from *Luminiphilus syltensis*, resolved by X-ray crystallography.[14] Herein, we refined the structure before the bioinformatic analysis to simulate the structure of the enzyme in the reaction medium. In this way, we could gain an accurate view of the active site's geometry and we prepared the quinonoid intermediates of the substrates of interest. The crystal structure contained six polypeptide chains associated in pairs to form a hexamer with a pyridoxal 5'-phosphate (PLP) molecule in each active site covalently bound to the catalytic lysine (K158). Possible conformations were sampled by a short (500 ps) molecular dynamics simulation (MD simulation) under the YAMBER3 force field at 25^{o}C, pH 7.5.

The refined structure was evaluated with MolProbity. The overall clashscore of the model was improved (0.58 compared to 6.37 in the crystallographic structure). Moreover, the

crystallographic structure before the refinement displayed 20 Ramachandran outliers while in the refined model, only V104 in chains B and F adopted sterically unreasonable φ and ψ values on the Ramachandran plot. Then, the Schiff base linkage in chain A of the hexamer was removed and the quinonoid intermediate of (*R*)-1-phenylethylamine was built. The model was gradually energy minimized. However, the resulting model was incompatible with the experimentally determined physical requirements of the quinonoid complex since the pyridine of the PLP cofactor was significantly distorted (**Figure 11A**). We hypothesized that since the target model resembles not the initial resting state but an intermediate along the reaction coordinate, the MD stimulations should start with a structure of the cofactor in the intermediate state. The fact that we simulated the movement of the protein with the cofactor in the internal aldimine state naturally samples low energy structures with active site conformations closer to the resting state of the enzyme and thus with low complementarity to the substrate-cofactor complex. This could explain why the resulting structure had no preference to bind the substrate and the energy minimization forced the substrate-cofactor complex to get an abnormal conformation.

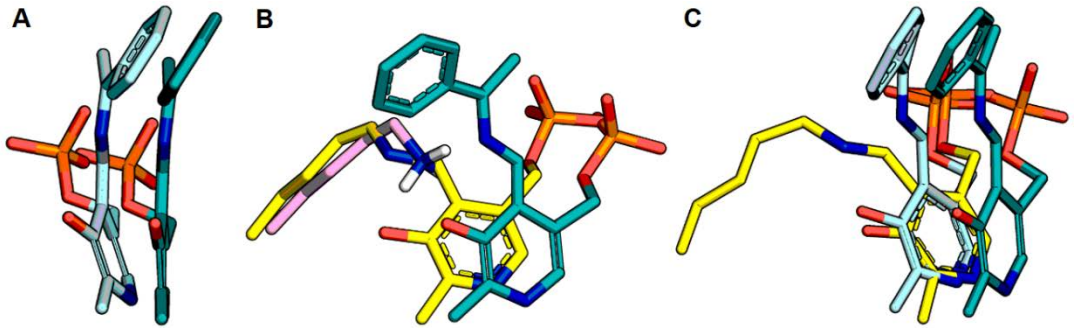

Figure 11. Differences between the cofactor in the internal aldimine (yellow) crystallographic structure and the quinonoids of (*R*)-PEA in the two models generated from MD simulations. **A:** the bend structure of the quinonoid intermediate of (*R*)-PEA in cyan is an artifact of the initial MD stimulation. The structure on the right (teal) represents the same quinonoid intermediate that resulted from the second MD experiment **B:** the relative position between of the internal aldimine in the initial crystal structure and the positions of the catalytic Lys (pink) and the quinonoid intermediate of (*R*)-PEA (teal) after the second MD stimulation. **C:** overlay of all the cofactor complexes between the 3 models. The internal aldimine model from the crystallographic data after refinement (yellow), the quinonoid after the first (cyan) and the second (teal) MD experiment.

We therefore run the MD stimulation again but this time we constructed the quinonoid intermediate of isopropylamine (IPA) in the active site before starting the experiment. Isopropylamine was chosen instead of the phenylalkylamine target substrates because

placing a bulky phenyl substituent in the active site during the simulation might limit the possible movements of the polypeptide. After the simulation, IPA was replaced with (*R*)-1-phenylethylamine and the structure was again gradually energy minimized as before.

This time the simulation was successful. The spatial organization of the active site was in line with other experimentally determined structures of the same fold type and is described in detail in the next section (section 3.3).[9] Moreover, the model reproduced the planar conformation of the quinonoid intermediate (**Figure 11A**).[24] The cofactor appeared to have slightly moved away from the catalytic lysine (**Figure 11B**). This movement of the cofactor between the two states is consistent with notion that enzymes are flexible templates and that mutual interactions between the enzymes functional groups and the substrate induce conformational change in the enzyme structure and thus in the cofactor position in the active site upon substrate binding. The overall protein structure has an RMSD value of 2.068 Å compared to the crystallographic structure so the resulting overall fold is close to the experimental one. After the simulations and the energy minimization the final hexameric model has better MolProbity clashscore (0.36 compared to 6.37) and less Ramachandran outliers (2 compared to 20). The two outliers, residues V104 and T269 were located in chain E. The rest of the polypeptide chains of the hexamer had no steric flaws.

3.3 Active site interactions

The model structure of the amine transaminase from *Luminiphilus syltensis* (LS_ATA) after the bioinformatic analysis described in section 3.2, provided an excellent opportunity to explore the active site conformation in the in the quinonoid intermediate step of the reaction cycle. Using PyMOL we investigated the nature and the arrangement of all the amino acid residues important for the coordination of the cofactor and the phenyl and methyl group of (*R*)-1-phenylmethylamine.

3.3.1 Cofactor binding

As shown in **Figure 12** all the main handles utilized to stabilize the cofactor in the active site described for (*R*)-selective amine transaminases (section 1.4),[9] exist in LS_ATA. First, the hydrogen bond network formed around the 5'-phosphate moiety creates a tight grip on the cofactor. The 5'-phosphate group participates in five hydrogen bonds with the side chains of residues T249, R54, T213 and with the backbone nitrogen atom of I212 (Pi "Binding Cup"). Then, the protonated pyridine nitrogen atom is hydrogen

bonded to the γ-carboxylate group of a conserved glutamate residue (E187). Additionally, the guanidino group of R158 is located 3,5 Å away from the 3'-oxygen atom of the pyridine ring and possibly coordinates it through a water molecule. The catalytic lysine residue (K154) is in close physical proximity (3.6 Å) to the PLP ring.

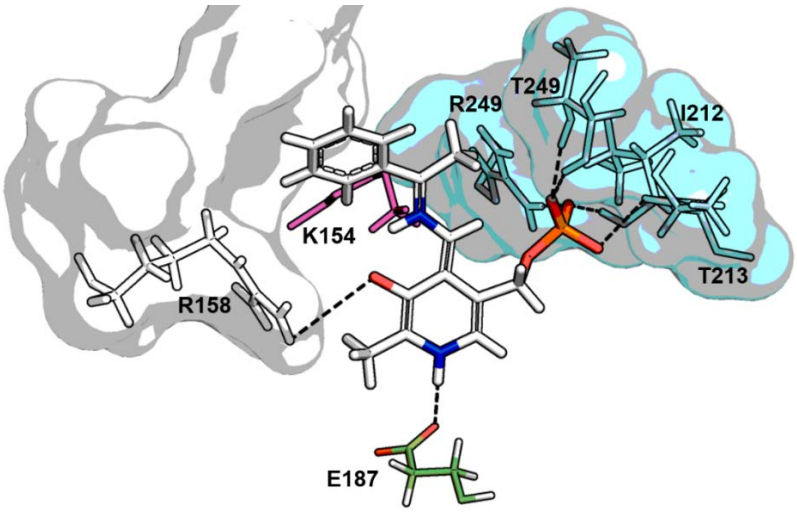

Figure 12. Depiction of the amino acid residues that are important for cofactor stabilization in the active site of LS_ATA. The PLP cofactor is presented with (*R*)-PEA bound in the quinonoid conformation in sticks (elemental coloring, carbons in white). The view is from the *si* face of the cofactor plane. Multiple hydrogen bonds (dashed lines) prevent the cofactor from dissociation. Residues in the cyan colored surface form the Pi "Binding Cup". E187 (elemental coloring, carbons in green) coordinates the pyridine nitrogen atom and R158 the 3'-oxygen atom of the cofactor. Note that R158 belongs in the large substrate binding pocket (white surface) that will also be discussed in the next section. When the holoenzyme is in its resting state the carbonyl moiety of the PLP cofactor also forms a Schiff base with the catalytic lysine (K154).

3.3.2 The two-pocket substrate binding site

As expected for (*R*)-selective transaminases, the large pocket of the amine transaminase from *Luminiphilus syltensis* (LS_ATA) is located directly above the 3'-pyridine oxygen of the cofactor while the small pocket is located above the 5'-phosphate group (**Figure 13**). Residues F35 and R92 from the βX and the βY sheets of the N-terminal domain, L30* from the second subunit and R158 from the C-terminal domain, frame the large binding cavity from three sides (**Figure 14**). Residues F35, L30* are hydrophobic while the two arginine residues (R92 and R158) are polar, which confirms that the large binding pocket is responsible for dual substrate recognition, as observed in (*R*)-ATAs. On the opposite side, above the 5'-phosphate group of the cofactor lies the small binding pocket which is laid out by the three amino acid residues A250, S248, T249 of a β-turn of the C-terminal domain and residue V37A of the βX sheet of the N-

terminal domain. The entrance to the substrate binding site is defined by the interdomain loop and a loop from the second subunit.

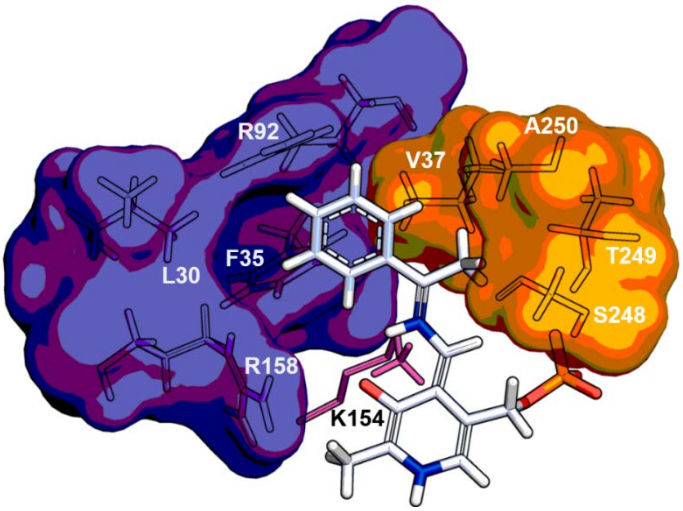

Figure 13. View of the large and the small binding pockets in LS_ATA in purple- and orange-colored surfaces, respectively, from the *si* face of the cofactor plane. The PLP is presented with (*R*)-PEA bound in a quinonoid conformation in sticks (elemental coloring, carbons in white), The catalytic lysine (K154) is shown in pink sticks.

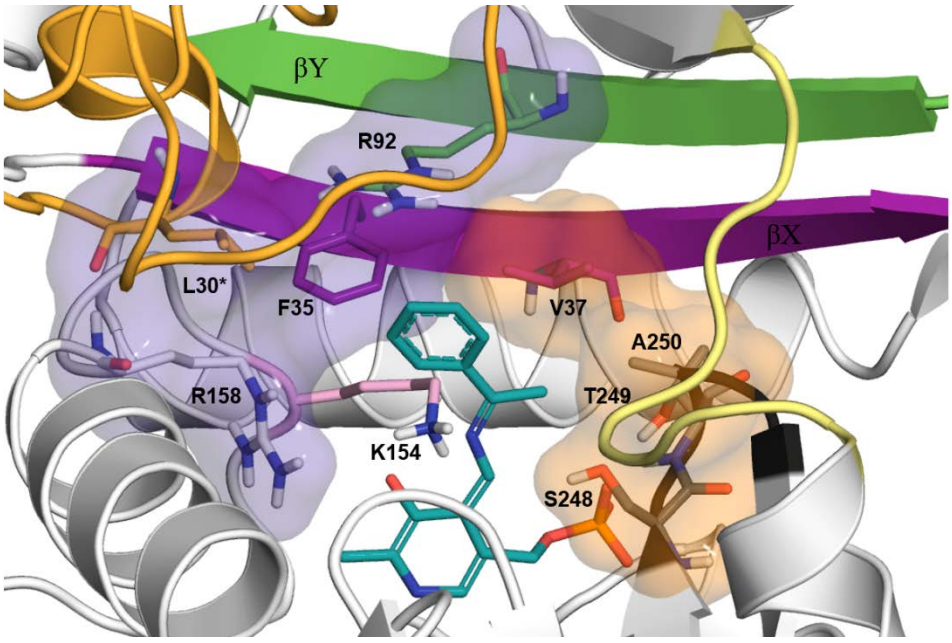

Figure 14. View of the active site of LS_ATA. The large binding pocket (purple) and the small binding pocket (orange) are shown, as well as the secondary structure elements of the protein in the vicinity of the substrate-cofactor complex. The βX and βY strands are colored in magenta and green, respectively. The interdomain loop is colored yellow and the β-turn in black. The cofactor with (*R*)-PEA bound (teal sticks, no hydrogens) and functionally important side chains are drawn in sticks (colored as the secondary structure, only polar hydrogens). The adjacent subunit is depicted in orange cartoon.

3.4 Formation energy of the (*R*)- and (*S*)-PEA quinonoids

The preference of the amine transaminase from *Luminiphilus syltensis* (LS_ATA) for the (*R*)-enantiomer was also verified *in silico* for the constructed model. YASARA FormEnergy command calculates the heat released or absorbed (formation enthalpy) during the formation of the target molecule from its elements based on semiempirical quantum chemistry methods.

The formation energies for the (*R*)- and the (*S*)-enantiomer of 1-phenylethylamine bound on pyridoxal 5'-phosphate (PLP) in the quinonoid intermediate state were -1521.65 kJ/mol and -1497.861 kJ/mol respectively.[14] The quinonoid of the (*R*)-enantiomer is thus favored by enthalpy. The energies are comparable because both quinonoid molecules are built from the same atoms. The enthalpy contributions cannot account alone for the binding energy of the substrates.[48] However, a complete thermodynamic study of the enzymes enantioselectivity is beyond the scope of this study. Entropy factors may be considered negligible for two reasons. First, both enantiomers are significantly restricted in the enzymes active site and secondly the cofactor is tightly bound to the apoenzyme which limits the degrees of freedom of the substrate-cofactor complex. A more detailed way to study receptor-ligand interaction are molecular docking studies. However, docking experiments are time consuming and this calculation here served more as a way of assessing that the resulted model from the MD stimulation is valid and less as a quantitative prediction of enantioselectivity.

3.5 Steric hindrances in the small binding pocket

Through MD simulations we managed to generate a model of the amine transaminase from *Luminiphilus syltensis* (LS_ATA) and the pyridoxal 5'-phosphate (PLP) cofactor in the quinonoid state with (*R*)-PEA bound.[14] The PyMOL script 'show_bumps' was used to pinpoint the residues in the small binding pocket whose atoms van den Waals radii overlap with the substrate's alkyl-substituent (**Figure 15**). Overlaps (bumps) are represented by disks of growing size ranging from green to red as the atom-pair radii overlap intensifies. The methyl group of (*R*)-PEA, the benchmark substrate, exerts no significant steric hindrance in the active site. Two small green bumps exist between the residues of the β-turn (S248, T249, A250). Elongation of the alkyl chain of the substrate by one methyl group and energy minimization of the system, yields (*R*)-PPA's quinonoid intermediate model structure. The ethyl substituent causes clashes with side chains of V37 and S248. Even more so, the butyl group of (*R*)-PBA's quinonoid, displays clashes

with multiple residues, namely V37, T249, A250. Based on the above observations we assumed that by mutating positions 37, 248 and 249 to alanine we could “excavate” the active site (section 1.9) and alleviate the steric barrier that blocks the binding of (*R*)-phenylethyl- and (*R*)-phenylbutylamine.

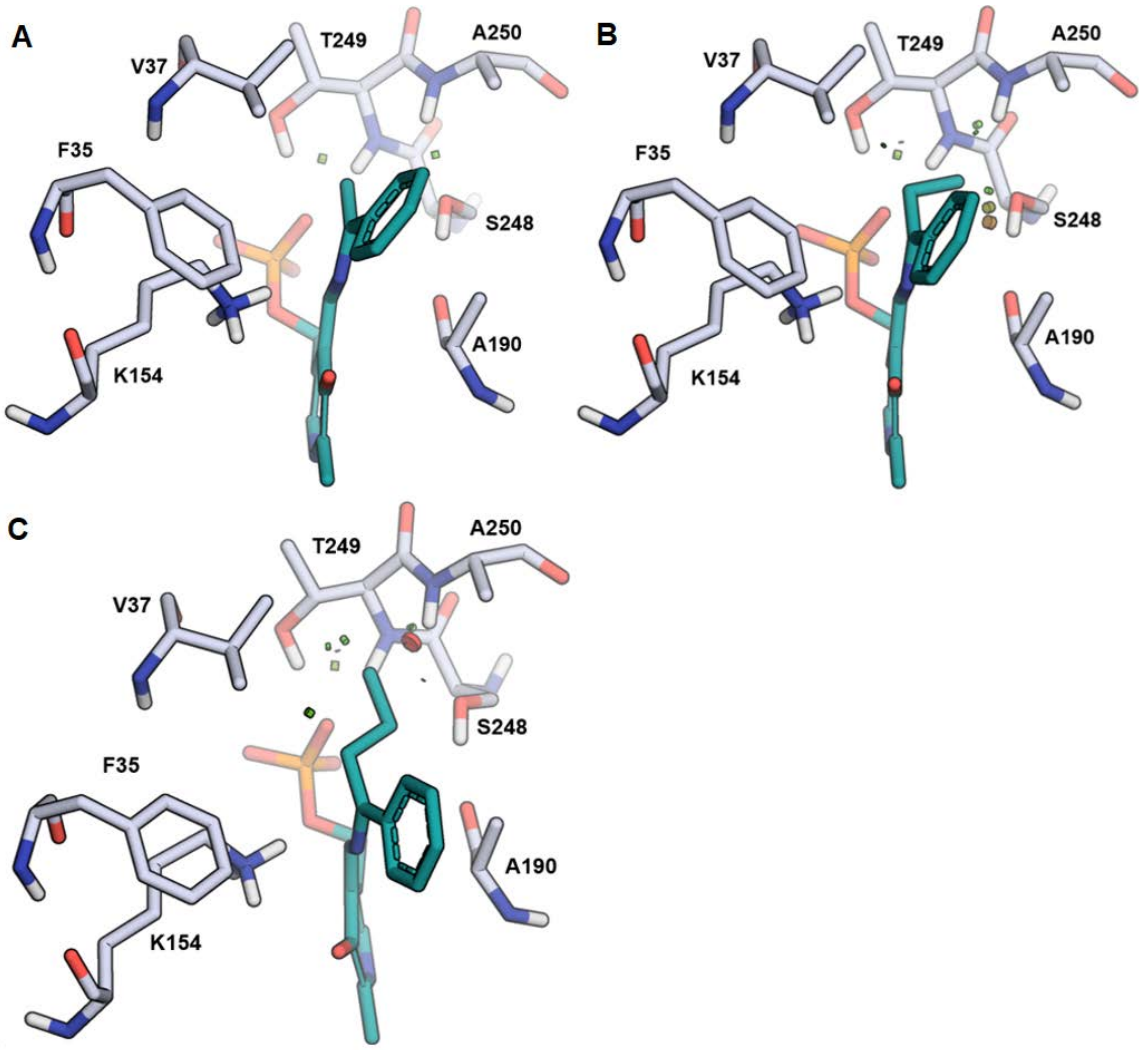

Figure 15. Quinonoids of **(A)** (*R*)-PEA, **(B)** (*R*)-PPA, **(C)** (*R*)-PBA in the small binding pocket. All three compounds were modelled and energy-minimized in silico in the active site of LS_ATA. The quinonoid is shown in sticks (teal). Residues within 4 Å of the alkyl substituent are shown as sticks (white). Some residues of the large binding pocket were omitted for clarity. Steric clashes (bumps) are shown in disks. The larger the alkyl chain, the more bumps appear in the small binding pocket.

3.6 Preparation of the constructs

Our goal was to create the single mutant LS_ATA variants V37A, S248A, T249A but also investigate the combined effect of these mutations on enzyme function. Site-

directed mutagenesis using primers with the appropriate mismatched nucleotide bases readily created the three single mutants which were then used as template sequences for the creation of the double mutants. The double mutated sequences V37A/S248A and V37A/T249A were produced. However, we failed to introduce two consecutive mutations in the positions that code for S248 and T249 in the parental sequence. We designed a double primer in which the codons that are complementary to those two positions of the parental stand, both code for alanine so that there would be less mismatches when the single mutant sequences (either S248A or T249A) were used as templates. PCR reactions were performed in two annealing temperatures (65^{o}C and 70^{o}C) but they were all unsuccessful. When the V37A/S248A mutant was used as a template sequence with the primer sequence coding for T229A at 65^{o}C annealing temperature, the reaction was successful. Sanger sequencing confirmed the triple mutant construct. Unfortunately, the triple mutant plasmid had a random mutation of a glycine to arginine residue along its coding sequence. Since the double mutants showed limited initial activity in the photometric assay (section 3.8) we did not perform additional experiments to synthesize the triple mutant again. All reaction mixtures after PCR were loaded on agarose gels and separated. Amplified plasmid products produce a single visible band as shown in **Figure 16**. The DNA of those samples is then treated with DpnI, transformed into TOP1O and BL21 *E.coli* cells as described in sections 2.4 and 2.5 before the construct can be verified by Sanger sequencing.

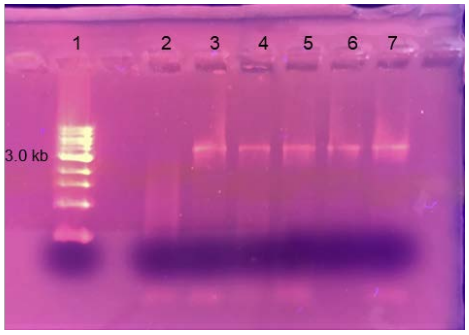

Figure 16. Agarose 0.8% ($^{w}/_{w}$) electrophoresis stained with EtBr. The first lane contains the 1 kb marker. The rest of the lanes contain the amplified plasmids of the single mutants V37A (lane 3), S248A (lane 4, 5) and T249A (lane 6, 7), except for the second lane where the PCR reaction failed and a smear of the unreacted dNTPs is visible. The dark purple smear at the bottom of the gel is caused by the sample loading dye.

3.7 Expression level of the mutant genes

All variants, created with mutagenesis PCR, were expressed and purified in soluble form. However, the expression level of the variants compared to the wild-type enzyme decreased. On average, we obtained 25-30 mg of purified protein for the WT LS_ATA from 0.5 L liquid cultures of *E. coli* BL21 (DE3) cells in LB media, 16-18 h after induction, at 20^{o}C. Cultures of *E. coli* BL21 (DE3) cells harboring the mutant genes reached comparable densities 16-18 h after induction to cells harboring the WT enzyme under the same conditions, but the protein yield of the variants in soluble form after purification was only 3-4 mg per 0.5 L of liquid culture.

3.8 Activity improvements toward arylalkylamines

The variants and the wild-type enzyme of the amine transaminase from *Luminiphilus syltensis* (LS_ATA) were screened with the photometric assay developed by Schätzle et al..[37] Mutations in positions 37 and 249 decrease almost 2-fold the activity towards the deamination of the benchmark substrate, (*R*)-PEA (**Table 3**).[14] However, the V37A variant exhibited activity towards (*R*)-PPA, while the WT has no detectable activity with this assay. Mutation of both positions (37 and 249) to alanine also leads to a detectable activity towards (*R*)-PEA. When mutation S248A is introduced, the variants are inactive. No variant showed detectable activity towards the deamination of (*R*)-PBA with this assay.

Table 3. Specific activity [mU mg^{-1}] of purified LS_ATA mutants. Assay conditions: (*R*)-amine (1 mM) and pyruvate (2 mM) at HEPES buffer (50 mM, pH 8.0, 0.05 mM PLP), 5% $^{v}/_{v}$ DMSO, 0.6-1.2 mg mL^{-1} purified enzyme.

LS_ATA variant	(*R*)-PEA [mU mg^{-1}]	(*R*)-PPA [mU mg^{-1}]
Wild type	274 ± 54	n.a
V37A	93 ± 16	45 ± 26
S248A	n.a$^{\alpha}$	n.a
T249A	138 ± 36	n.a
V37A/S248A	n.a	n.a
V37A/T249A	n.a	1.8 ± 0.7

$^{\alpha}$ n.a, not active or below the detection limit

The photometric assay revealed that mutation V37A has a beneficial influence in the acceptance of bulkier substituents, and thus, this variant was used for further experiments. Residues S248 and T249 are in close proximity with phosphate group of PLP, which possibly explains the reduction or total loss of activity observed. This hypothesis was further tested in the pyridoxamine 5'-phosphate formation assay, described in the next section (section 3.9). Identifying a single mutant (V37A) though a rationally designed alanine scanning process that displayed activity towards (*R*)-PPA was quite straight forward, compared to the engineering efforts in the small binding pocket in (*S*)-ATAs, which have been more laborious.[41,49,50,51] A reason for this is that the small binding pocket in (*R*)-ATAs is secluded from the homodimer interface, while the opposite is true for (*S*)-ATAs. Höhne et al. tried a similar strategy of excavating the small binding pocket of the (*S*)-selective ATA from *V. fluvialis* without success,[15] because the residues in the vicinity of the small methyl substituent are mainly placed in loops in the interface of the homodimer and have additional functional roles in protein flexibility and stability.

3.9 PMP formation is not observed in the inactive variants

Unfortunately, the S248A, V37A/S248A, V37A/T249A variants showed no activity in the photometric assay, even with the benchmark substrate, (*R*)-PEA (section 3.8). Although we observed no product formation, it was yet possible that the variants do bind and deaminate the amine substrate, form pyridoxamine 5'-phosphate (PMP) in their active site, but cannot bind the amine acceptor, pyruvate, in order to complete the reaction cycle. The PMP formed in the end of the first-half reaction can be detected photometrically, as it absorbs in different wavelengths compared to the PLP or its internal aldimine. The initial E-PLP (internal aldimine) complex in the wild-type LS_ATA at pH 9.0 has an absorption maximum centered at 410 nm (**Figure 17**). This is line with the absorbance maxima of the internal aldimine observed for other fold class IV enzymes.[52] Upon incubation with (*R*)-PEA the color of the solution shifts from pale-yellow to colorless, consistent with the conversion of the internal aldimine to PMP, which absorbs at 330 nm. The internal aldimine configuration absorption band of the mutants is slightly shifted compared to the wild-type enzyme and is centered around 400 nm.[14] They also exhibit a second less intense peak at 320-330 nm, which could be attributed to the second tautomeric form of the protonated Schiff base of the internal aldimine (**Figure 18**). This enolimine tautomer is considered to be a less reactive species for the nucleophilic attack by the amine substate. Different spatial organization of polar amino

acids in the vicinity of the cofactor in the active sites of the wild-type and the variant enzymes can affect the pKa of the imine nitrogen and different hydrogen bonding networks can affect the tautomerism of the Schiff base. For example, it has been shown that the solvation of the 3'-oxygen favors the ionic form of the oxygen moiety and moreover the protonation of the pyridine nitrogen stabilizes the 3'-O negative charge in the pyridine ring, making the ketoenamine external aldimine the dominant species in the active site of aspartate aminotransferase.[53] No spectral shift at 330 nm was detected for the V37A/S248A, V37A/T249A variants upon incubation with (*R*)-PEA indicating that the amine substrate is not accepted in the active site. For the S248A variant, a moderate peak at 330 nm indicating PMP formation is detected, however a large proportion of the enzyme remains in the internal aldimine form.[54,55]

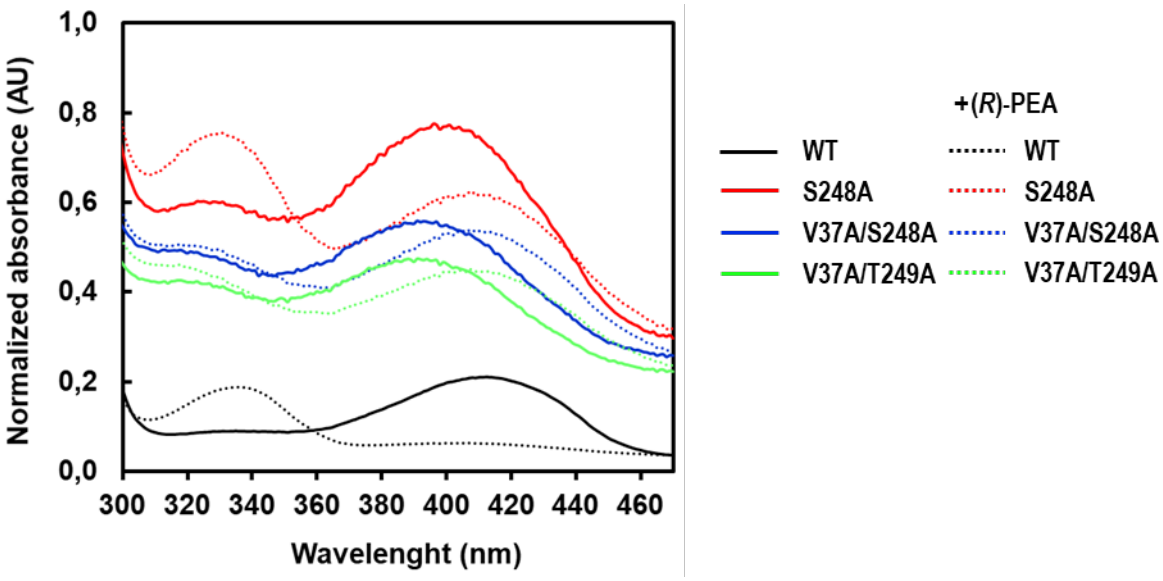

Figure 17. The UV absorbance spectra for the transamination half-reaction of LS_ATA wild-type (black) enzyme and the variants (S248A, red; V37A/S248A blue; V37A/T249A green) that displayed no activity in the photometric assay. Solid lines represent the spectra of the internal aldimine while dashed lines represent the spectra upon addition of (*R*)-PEA.

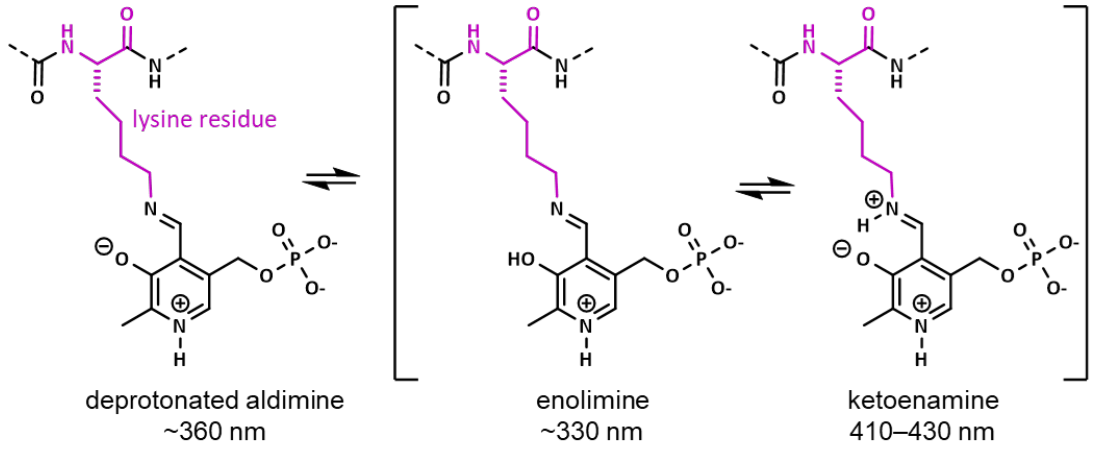

Figure 18. Structures of the different ionic and tautomeric forms of the internal aldimine.

3.10 The effect of pH on enzyme activity and stability

It is well documented that amine transaminases have a higher activity at alkaline pH solutions, for example a pH optimum of 8.5 for the (*R*)-selective ATA-117[38] and of 9.2 for the (*S*)-selective ATA from *Vibrio fluvialis*[56] has been reported. Therefore, we studied the initial velocity of the overall transamination reaction of (*R*)-PEA and pyruvate catalyzed by the wild-type and the V37A variant over the pH range 8-10 (**Figure 19**). Unexpectedly, the V37A variant showed higher specific activity than the wild-type above pH 9.0. The overall trend of the pH-curve is the same for both enzymes as the activity rises with the rising proton concentration of the solution. Both enzymes show maximum initial velocity towards (*R*)-PEA at pH 10, with specific activities of 537 ± 11 mU mg^{-1} and 374 ± 3 mU mg^{-1} for the V37A variant and the wild-type, respectively. This means that a larger fraction of the enzyme is in its catalytically active ionization state at pH 10 compared to lower pH solutions. The most important ionizable group for the transamination reaction is the ε-amino group of the catalytic lysine in the active site. A pH of 10 is close to the pK_a of lysine and may thus favor lysine to act as an acid/base during catalysis. The question however remains as to why a single mutation renders the V37A variant more active than the wild-type in higher pH solutions.

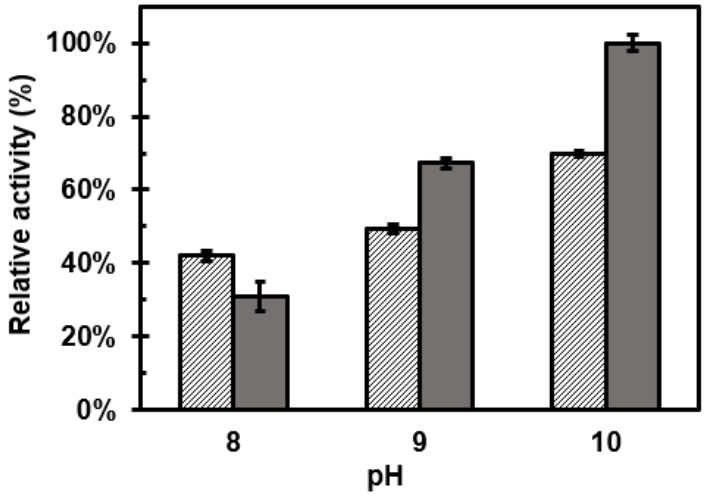

Figure 19. pH-initial rate profile of wild-type (striped columns) and the V37A variant (grey columns) for the transamination of (*R*)-PEA (1 mM) and pyruvate (2 mM). The reaction took place in 25 mM of the appropriate buffer with 0.05 mM PLP at 25 ^{o}C. HEPES buffer was used for pH 8.0 and CHES buffer for pH 9.0 and 10.0.

Incubation of both the V37A variant and the wild-type enzyme has moderate effects on the stability of the enzymes (**Figure 20**). Both enzymes were incubated without substrate in the same buffered solutions of pH 8.0, 9.0 and 10.0 for 24 h, 25^{o}C and the initial velocities against (*R*)-PEA with pyruvate as the amine acceptor were measured with the photometric assay. It was observed that at pH 8.0 and 9.0, the enzymes retained 100 % of the initial activity after incubation for 24 h. In fact, incubation of the enzymes for 5-7 h at pH 8.0 or 9.0 even leads to a hyperactivation. This activation effect is not observed when the enzymes were incubated at pH 10. Incubation at pH 10 leads to 20-30% loss of activity for both enzymes after 24 h. However, this loss of activity is due to the instability of the cofactor at pH 10, because addition of fresh PLP after 7 h of incubation fully restored the activity of the V37A variant. The rate of hydrolysis of aldimine bonds between PLP and amino acids in aqueous solutions is pH dependent and is greatly enhanced at pH 10.[57] Due to the higher dissociation rate of the cofactor at pH 10 we chose to use a buffer of pH 9.0 for further experiments in order to avoid the need to add PLP during the course of the reaction.

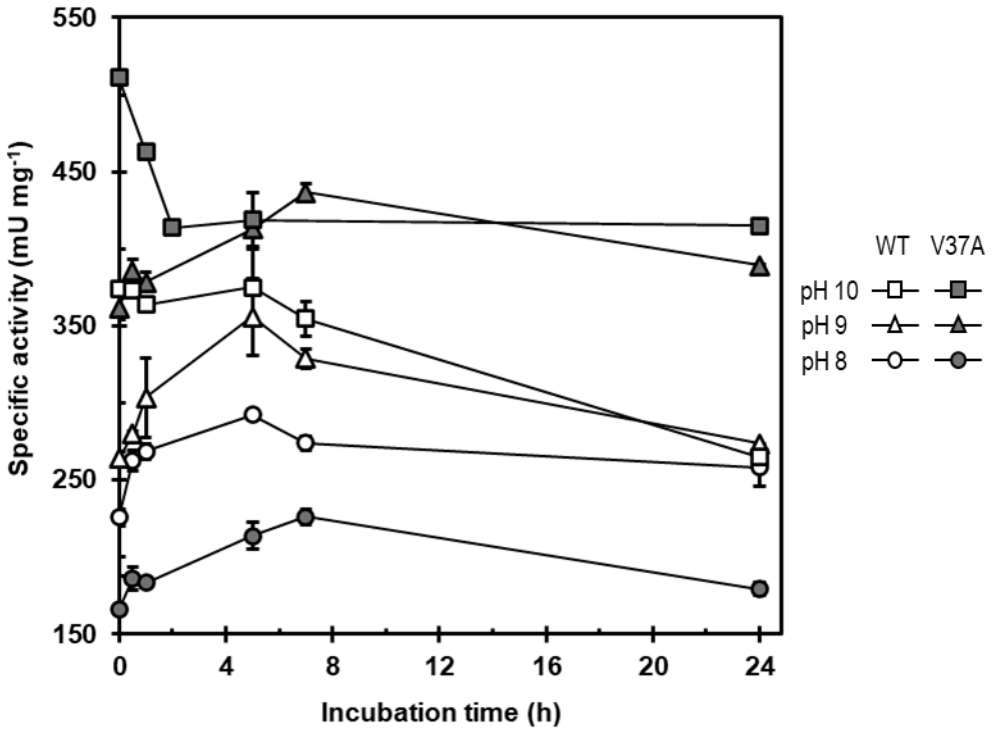

Figure 20. pH-initial rate profile after incubation of wild-type (white elements) and the V37A variant (grey elements) for 24 h, 25 ^{o}C in three different pH buffered solutions. HEPES buffer was used for pH 8.0 (circles) and CHES buffer for pH 9.0 (triangles) and 10.0 (squares). Samples of the incubated enzymes were removed at various time points and the rate of the enzyme catalyzed reaction of (*R*)-PEA (1 mM) and pyruvate (2 mM) was measured photometrically.

3.11 Kinetic resolution of racemic amines

We applied the variant V37A and the wild-type amine transaminase *from Luminiphilus syltensis* (LS_ATA) for a semi-preparative scale kinetic resolution of racemic amines using pyruvate as the amine acceptor (**Figure 21**).[14] Reactions were performed at 35^{o}C in CHES buffer pH 9.0. Both the V37A variant and the WT LS_ATA fully converted the (*R*)-enantiomer of the benchmark substrate, (*R*)-PEA, in 3 h. The (*S*)-enantiomer remained unreacted throughout the 24 h that the reaction was monitored (ee_s 100% for both enzymes after 24 h) highlighting the high enantioselectivity of amine transaminases. Despite the lack of activity in the photometric assay, the wild type exhibited activity with the (*R*)-PPA, with a 20% conversion after 24 h. The V37A had a better catalytic performance towards the conversion of (*R*)-PPA, reaching at the same conversion in 2 h.

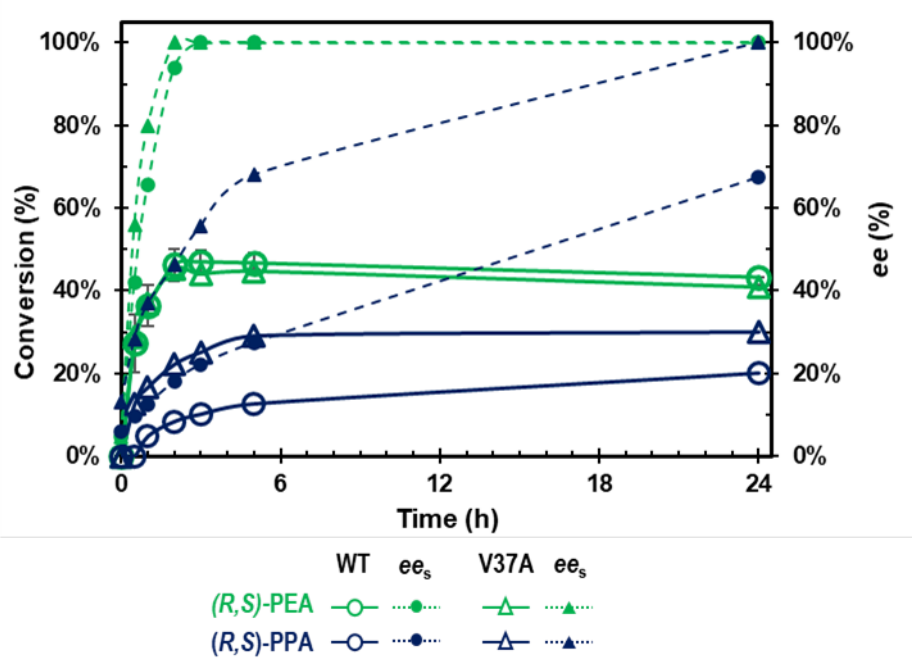

Figure 21. Kinetic resolution of (*R,S*)-PEA (green) and (*R,S*)-PPA (blue) by the wild-type LS_ATA (circles) and the V37A variant (triangles). The empty schemes denote % conversion and the filled ones the ee_s. The reactions were performed in a 2 mL scale with 0.06 mg of each enzyme, 8 mM racemic amine, 16 mM pyruvate, CHES buffer (pH 9.0, 50 mM), 0.1 mM PLP, 5% DMSO, 35°C, 750 rpm.

Since the acceptance of 1-PPA from the wild-type LS_ATA was not detected in the photometric assay we were encouraged to investigate the ability of the wild-type and the V37A variant to deaminate 1-phenylbutylamine (**Figure 22**). Racemic 1-PBA was not available so we performed the reaction in kinetic resolution mode with (*R*)-PBA and pyruvate. The variant V37A displayed activity towards (*R*)-PBA, reaching to almost full conversion of the substrate after 24 h. The wild type displayed insignificant activity (~3% conversion in 24 h).

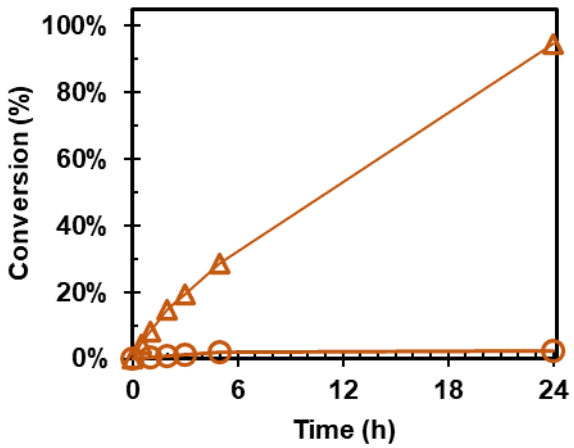

Figure 22. Deamination of (*R*)-PBA by the wild-type LS_ATA (circles) and the V37A variant (triangles). The reaction was performed in a 2 mL scale with 0.06 mg of each enzyme, 4 mM of enantiopure (*R*)-PBA, 8 mM pyruvate, CHES buffer (pH 9.0, 50 mM), 0.1 mM PLP, 5% DMSO, 35^{o}C, 750 rpm.

The reason why the activity of the wild-type LS_ATA towards (*R*)-PPA and the activity of the V37A variant towards (*R*)-PBA was not detected with the photometric assay is not clear. Starting from the amount of product produced after 1 h of reaction and calculating the theoretical value of specific activity for this reaction (U mg^{-1}), assuming that the initial velocity remains constant throughout the reaction, we calculated that this activity could be well detected in the photometric assay. A possible explanation stems from the fact that the substrate concertation was different between the two reactions (1 mM of enantiopure amine in the photometric assay and 4 mM in the kinetic resolution reaction). Due to the hyperbolic relationship between the enzyme's initial velocity and the substrate concentration, if the apparent K_M concerning the amine substrate is in the mM range, then the fraction of the V_{max} observed at 1 mM substrate would be significantly lower.

3.12 Asymmetric synthesis of chiral amines

We tried to apply four different methodologies for the asymmetric synthesis of the (*R*)-enantiomer of the alkylamines that were successfully converted in kinetic resolution mode using 0.07 mg of the purified V37A variant. First, we used isopropylamine (IPA)[38]in great excess (100 to 750 mM) and 8 mM of the ketone (acetophenone, propiophenone or butyrophenone) in CHES buffer with 5% ($^{v}/_{v}$) DMSO, pH 9.0, 35^{o}C. The enzyme shows no activity towards IPA, and was unable to synthesize the corresponding amine. Using the same reaction conditions we used *p*-xylylenediamine (3

equivalents) as amine donor. Deamination of one of the amine groups could lead to Schiff base formation and precipitation of the co-product. This removal of the co-product could shift the equilibrium, as it happens is the case of o-xylylenedimine[34,35] However, this reaction was also unsuccessful. We even performed the reaction with equimolar amount of (*R*)-PEA as amine donor for the amination of butyrophenone the reaction only produced trace amounts of (*R*)-1-phenylbutylamine. Lastly, we used D-alanine as the amine donor coupled with lactate dehydrogenase (LDH) and glucose dehydrogenase (GDH), in order to convert pyruvate to lactate, which is another common strategy to shift the equilibrium[31] The reaction was again unsuccessful, even when we used almost ten times the amount of enzyme (0.6 mg) used in kinetic resolution of 1-PBA. The asymmetric synthesis of the (*R*)- or the (*S*)-enantiomer of 1-phenylethylamine catalyzed by the wild-type LS_ATA and the amine transaminase from *Vibrio fluvialis* respectively using the LDH/GDH system, was performed successfully as a positive control.

CHAPTER 4

Conclusions

The (*R*)-selective amine transaminase from *Luminiphilus syltensis* (LS_ATA) was engineered in order to widen the small binding pocket for hosting the bulky alkyl chain of *R*-1-phenylbutylamine ((*R*)-PBA). The wild-type exhibited insignificant activity towards this substrate but the incorporation of a single mutation (V37A) led to its effective acceptance. Identification of this single mutant was done rationally, through bioinformatic analysis. A MD simulation approach provided a model of the active site's conformation around the quinonoid intermediate structure of (*R*)-1-phenylethylamine, which is consistent with the physical and chemical requirements of the reaction mechanism. By elongating the substrate's alkyl chain from ethyl to butyl, unfavorable van der Waals contacts evolve in the small binding pocket which explains the reduced activity of the wild-type towards bulky phenyl amines. Three hotspots were identified for mutagenesis in order to excavate the small binding pocket. We performed site-directed mutagenesis, confirmed the constructs, expressed them and purified them and finally biochemically characterized them for the desired activity. The kinetic resolution method was used to assess the enantioselectivity of the variants. The most prominent mutant, V37A successfully deaminated PPA and PBA with pyruvate as the amine acceptor in preparative scale reactions. Variants caring the mutations S248 and T249 had reduced or no activity possibly because of the disruption of the hydrogen bond network around the 5'-phosphate moiety of the cofactor. This is supported by half transamination reaction experiments. Finally, the V37A was employed in asymmetric synthesis of (*R*)-PBA but despite our efforts to shift the unfavorable thermodynamic equilibrium based on known literature methods, no conversion was achieved.

Appendix I - Sequences

DNA sequence of LS_ATA wild-type gene, 906 bp

```
  1 atgtccgatg aaccgattat ttatattaat ggcgattatc tgccgctgag ccaggcacgt
 61 gtttctccgg ttgatcaggg ttttctgctg ggtgatggtg tttttgatgt tgttagcgcc
121 tggaaaggca atatttttaa actggatgcc catctggatc gttttttga tagcattcag
181 gcagcacgtc tgaatcatga tatgagccgt gatgcatgga aagaagccat tattgaaacc
241 acccgtcgta atggtctgga tgatgccagc attcgtttta ttgttacccg tggtgaaccg
301 aaaggtgttg ttgcagatcc gcgtgatttt aaaccgacct gtattgtttg ggttgcaccg
361 tatatttttc tggccgatga agaaaaacgt cgtaatggca ttcgtctgat gattagcgca
421 acccgtggtt ttccggcaga taccctggac cctcgttata aatgtctgga tcgtctgcat
481 agccagctga ttcgtctgga agcactggaa gccggttatg atgatgcact gtggctggat
541 catagcggtc atgttagcga aagcgcagca agcaacctgt ttattgtgaa aaatggcgtt
601 ctgtataccc cgagcgcagg tattctgcgt ggtattaccc gtgataccat tctggaactg
661 gcaaccgaac tggatattcc gtggaaagaa cgtcagctga gcgcatttga tgtttatatt
721 gccgatgaag tgtttacctg ttctaccgca ggcggtgcac tgccggttcg tgaagttgca
781 ggtcgtacca ttcgtggcac cacaccgggt ccgattaccc aggcaattga taatgcatat
841 tgggcaatgc gtgaaaccga tcgttatgca acaccgctgt caggatccca tcatcatcat
901 catcat
```

Amino acid sequence of LS_ATA wild-type, 302 aa

```
MSDEPIIYIN GDYLPLSQAR VSPVDQGFLL GDGVFDVVSA WKGNIFKLDA
HLDRFFDSIQ AARLNHDMSR DAWKEAIIET TRRNGLDDAS IRFIVTRGEP
KGVVADPRDF KPTCIVWVAP YIFLADEEKR RNGIRLMISA TRGFPADTLD
PRYKCLDRLH SQLIRLEALE AGYDDALWLD HSGHVSESAA SNLFIVKNGV
LYTPSAGILR GITRDTILEL ATELDIPWKE RQLSAFDVYI ADEVFTCSTA
GGALPVREVA GRTIRGTTPG PITQAIDNAY WAMRETDRYA TPLSGSHHHH
HH*
```

Appendix II - Chromatograms

Representative chromatograms for the kinetic resolution experiments are given below.

Reactions conditions: 0.06 mg enzyme, 8 mM racemic amine, 16 mM pyruvate, CHES buffer (pH 9.0, 50 mM), 0.1 mM PLP, 5% DMSO, in 2 mL scale 35^{o}C, 750 rpm.

LS_ATA wild type, resolution of (*R,S*)-PEA:

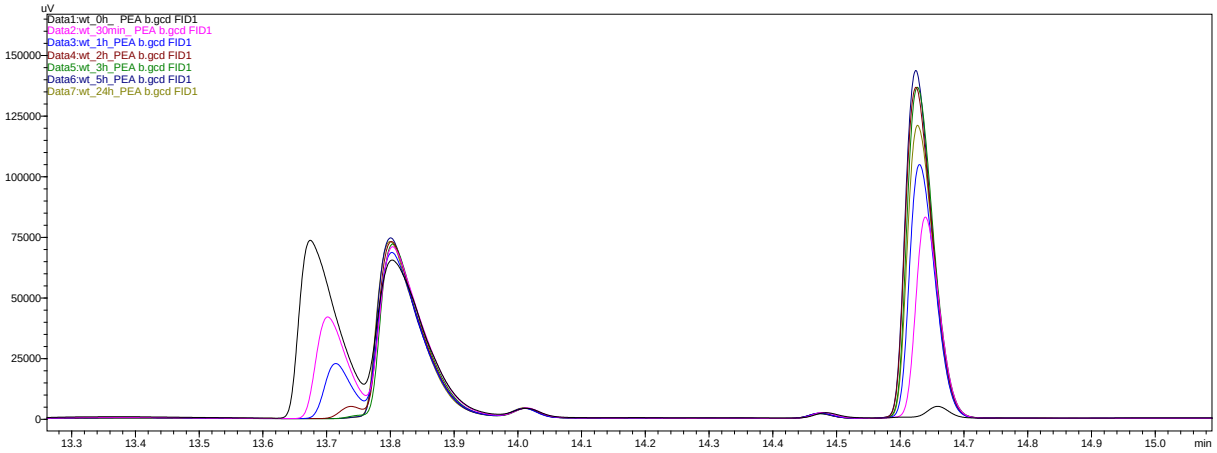

V37A variant, resolution of (*R,S*)-PEA:

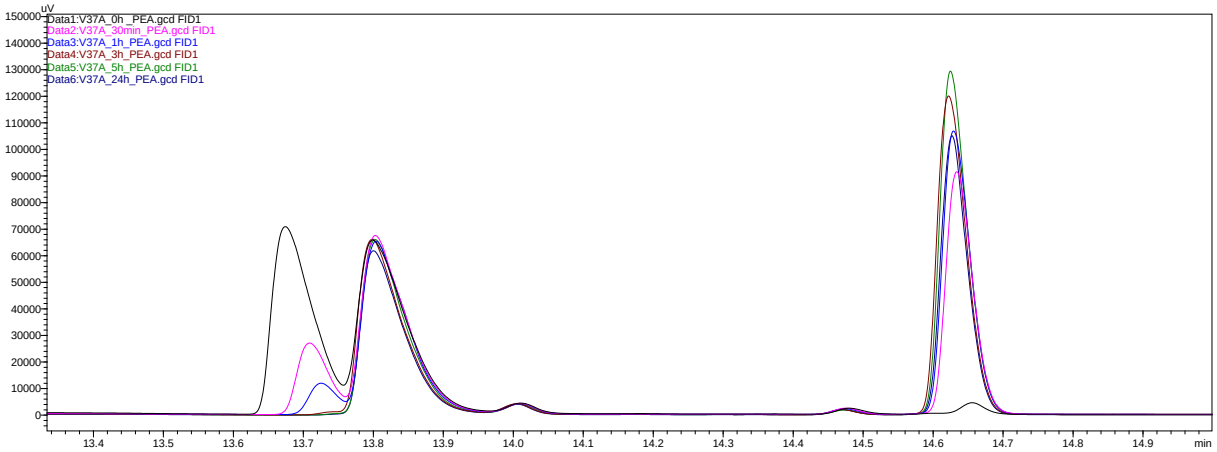

Compound	Retention Time (min)
(*R*)-phenylethylamine	13.8
(*S*)-phenylethylamine	14.0
acetophenone	15.4

LS_ATA wild type, resolution of (*R,S*)-PPA:

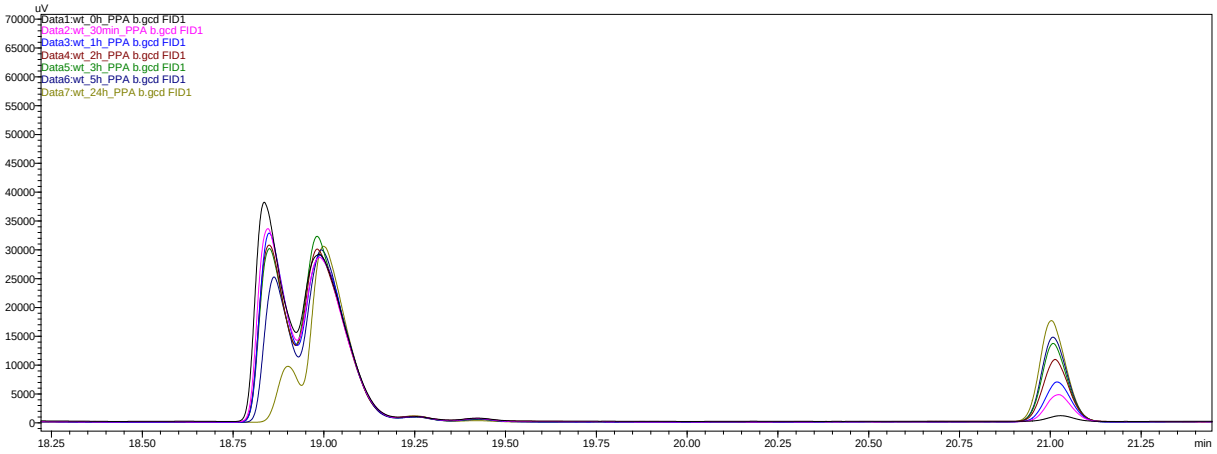

V37A variant, resolution of (*R,S*)-PPA:

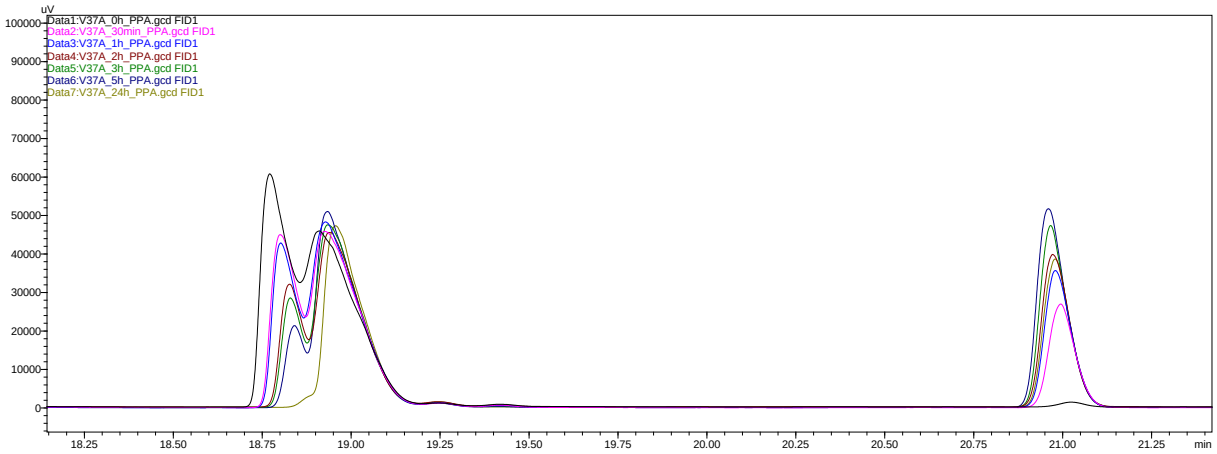

Compound	Retention Time (min)
(*R*)-phenylpropyllamine	18.7
(*S*)-phenylpropylamine	18.9
propiophenone	20.8

LS_ATA wild type, deamination of (*R*)-PBA:

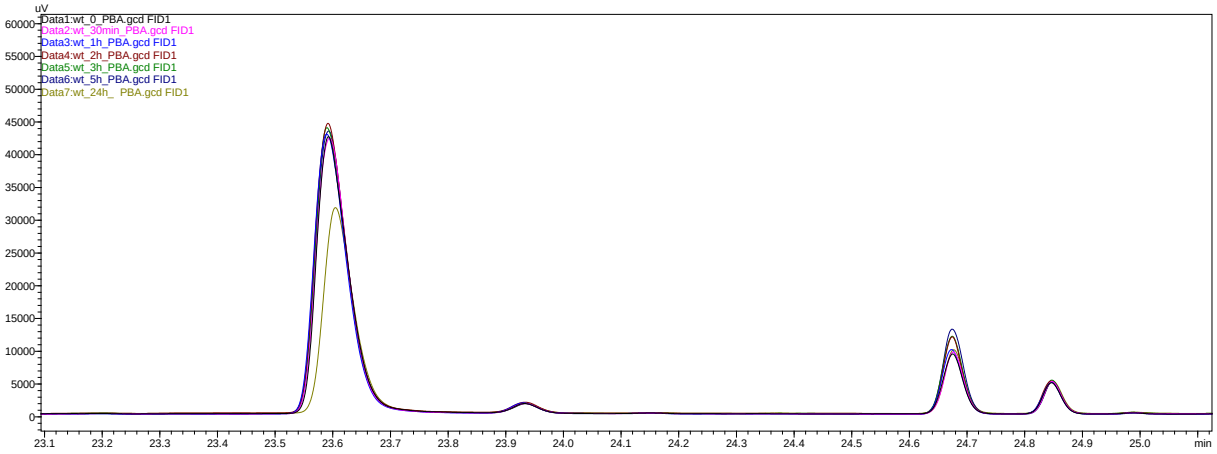

V37A variant, deamination of (*R*)-PBA:

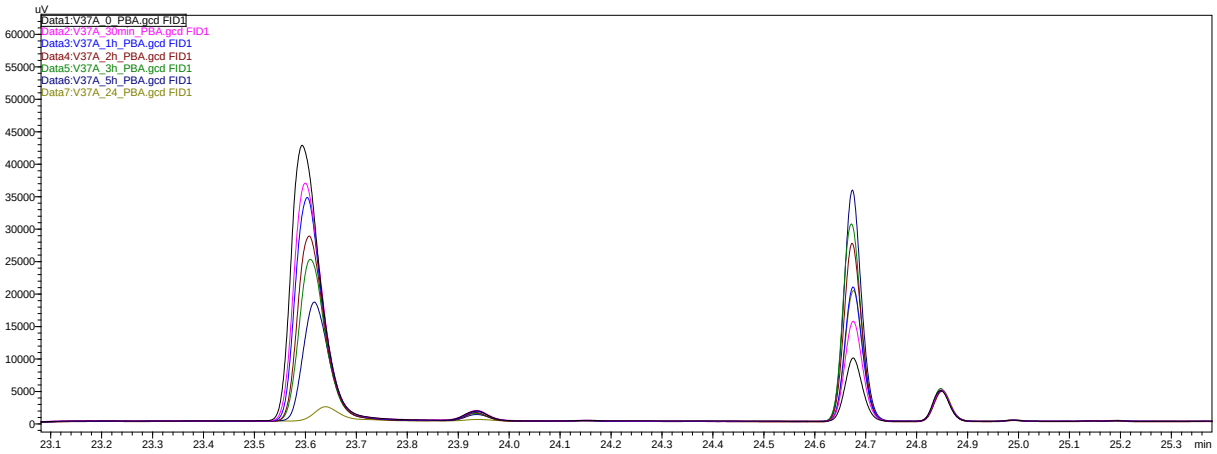

Compound	Retention Time (min)
(*R*)-phenylbutylamine	23.5
butyrophenone	24.6

Bibliography

(1) Höhne, M.; Bornscheuer, U. T. Application of Transaminases. In *Enzyme Catalysis Organic Synthesis Third edition*; Drauz, K., Gröger, H., May, O., Eds.; Wiley-VCH: Weinheim, 2012; pp 779–820.

(2) Calvelage, S.; Dörr, M.; Höhne, M.; Bornscheuer, U. T. A Systematic Analysis of the Substrate Scope of (S)- and (R)-Selective Amine Transaminases. *Adv. Synth. Catal.* **2017**, *359* (23), 4235–4243.

(3) Fuchs, M.; Farnberger, J. E.; Kroutil, W. The Industrial Age of Biocatalytic Transamination. *European J. Org. Chem.* **2015**, *2015* (32), 6965–6982.

(4) Simon, R. C.; Mutti, F. G.; Kroutil, W. Biocatalytic Synthesis of Enantiopure Building Blocks for Pharmaceuticals. *Drug Discov. Today Technol.* **2013**, *10* (1), e37–e44.

(5) Toney, M. D. Controlling Reaction Specificity in Pyridoxal Phosphate Enzymes. *Biochim. Biophys. Acta - Proteins Proteomics* **2011**, *1814* (11), 1407–1418.

(6) Percudani, R.; Peracchi, A. A Genomic Overview of Pyridoxal-Phosphate-Dependent Enzymes. *EMBO Rep.* **2003**, *4* (9), 850–854.

(7) Liang, J.; Han, Q.; Tan, Y.; Ding, H.; Li, J. Current Advances on Structure-Function Relationships of Pyridoxal 5′-Phosphate-Dependent Enzymes. *Front. Mol. Biosci.* **2019**, *6*, 4.

(8) Christen, P.; Mehta, P. K. From Cofactor to Enzymes. The Molecular Evolution of Pyridoxal-s'-Pliosphate-Dependent Enzymes. *Chem Record* **2001**, *1* (6), 436–447.

(9) Bezsudnova, E. Y.; Popov, V. O.; Boyko, K. M. Structural Insight into the Substrate Specificity of PLP Fold Type IV Transaminases. *Appl. Microbiol. Biotechnol.* **2020**, *104* (6), 2343–2357.

(10) Steffen-Munsberg, F.; Vickers, C.; Kohls, H.; Land, H.; Mallin, H.; Nobili, A.; Skalden, L.; van den Bergh, T.; Joosten, H. J.; Berglund, P.; Höhne, M.; Bornscheuer, U. T. Bioinformatic Analysis of a PLP-Dependent Enzyme Superfamily Suitable for Biocatalytic Applications. *Biotechnol. Adv.* **2015**, *33* (5), 566–604.

(11) Pollegioni, L.; Rosini, E.; Molla, G. Advances in Enzymatic Synthesis of D-Amino Acids. *Int. J. Mol. Sci.* **2020**, *21* (9), 3206.

(12) Inoue, K.; Kuramitsu, S.; Aki, K.; Watanabe, Y.; Takagi, T.; Nishigai, M.; Ikai, A.; Kagamiyama, H. Branched-Chain Amino Acid Aminotransferase of Escherichia Coli: Overproduction and Properties. *J. Biochem.* **1988**, *104* (5), 777–784.

(13) Zaitseva, J.; Lu, J.; Olechoski, K. L.; Lamb, A. L. Two Crystal Structures of the Isochorismate Pyruvate Lyase from Pseudomonas Aeruginosa. *J. Biol. Chem.* **2006**, *281* (44), 33441–33449.

(14) Konia, E.; Chatzicharalampous, K.; Drakonaki, A.; Muenke, C.; Ermler, U.; Tsiotis, G.; Pavlidis, I. V. Rational Engineering of Luminiphilus Syltensis (R)-Selective Amine Transaminase for the Acceptance of Bulky Substrates. *Chem. Commun.* **2021**, *57* (96), 12948–12951.

(15) Nobili, A.; Steffen-Munsberg, F.; Kohls, H.; Trentin, I.; Schulzke, C.; Höhne, M.; Bornscheuer, U. T. Engineering the Active Site of the Amine Transaminase from Vibrio Fluvialis for the Asymmetric Synthesis of Aryl-Alkyl Amines and Amino Alcohols. *ChemCatChem* **2015**, *7* (5), 757–760.

(16) Chen, S.; Berglund, P.; Humble, M. S. The Effect of Phosphate Group Binding Cup Coordination on the Stability of the Amine Transaminase from Chromobacterium Violaceum. *Mol. Catal.* **2018**, *446*, 115–123.

(17) Roura Padrosa, D.; Alaux, R.; Smith, P.; Dreveny, I.; López-Gallego, F.; Paradisi, F. Enhancing PLP-Binding Capacity of Class-III ω-Transaminase by Single Residue Substitution. *Front. Bioeng. Biotechnol.* **2019**, *7*, 282.

(18) Börner, T.; Rämisch, S.; Reddem, E. R.; Bartsch, S.; Vogel, A.; Thunnissen, A. M. W. H.; Adlercreutz, P.; Grey, C. Explaining Operational Instability of Amine Transaminases: Substrate-Induced Inactivation Mechanism and Influence of Quaternary Structure on Enzyme-Cofactor Intermediate Stability. *ACS Catal.* **2017**, *7* (2), 1259–1269.

(19) Shin, J. S.; Kim, B. G. Exploring the Active Site of Amine:Pyruvate Aminotransferase on the Basis of the Substrate Structure-Reactivity Relationship: How the Enzyme Controls Substrate Specificity and Stereoselectivity. *J. Org. Chem.* **2002**, *67* (9), 2848–2853.

(20) Steffen-Munsberg, F.; Vickers, C.; Thontowi, A.; Schätzle, S.; Meinhardt, T.; SvedendahlHumble, M.; Land, H.; Berglund, P.; Bornscheuer, U. T.; Höhne, M. Revealing the Structural Basis of Promiscuous Amine Transaminase Activity. *ChemCatChem* **2013**, *5* (1), 154–157.

(21) Dunathan, H. C. Conformation and Reaction Specificity in Pyridoxal Phosphate Enzymes. *Proc. Natl. Acad. Sci. U. S. A.* **1965**, *55* (4), 712–716.

(22) Höhne, M.; Schätzle, S.; Jochens, H.; Robins, K.; Bornscheuer, U. T. Rational Assignment of Key Motifs for Function Guides in Silico Enzyme Identification. *Nat. Chem. Biol.* **2010**, *6* (11), 807–813.

(23) Kirsch, J. F.; Eichele, G.; Ford, G. C.; Vincent, M. G.; Jansonius, J. N.; Gehring, H.; Christen, P. Mechanism of Action of Aspartate Aminotransferase Proposed on the Basis of Its Spatial Structure. *J. Mol. Biol.* **1984**, *174* (3), 497–525.

(24) Cassimjee, K. E.; Manta, B.; Himo, F. A Quantum Chemical Study of the ω-Transaminase Reaction Mechanism. *Org. Biomol. Chem.* **2015**, *13* (31), 8453–8464.

(25) Manta, B.; Cassimjee, K. E.; Himo, F. Quantum Chemical Study of Dual-Substrate Recognition in ω-Transaminase. *ACS Omega* **2017**, *2* (3), 890–898.

(26) Toney MD. Aspartate Aminotransferase: An Old Dog Teaches New Tricks. *Arch. Biochem. Biophys.* **2014**, *544*, 119–127. https://doi.org/10.1016/j.abb.2013.10.002.Aspartate.

(27) Mugford, P. F.; Wagner, U. G.; Jiang, Y.; Faber, K.; Kazlauskas, R. J. Enantiocomplementary Enzymes: Classification, Molecular Basis for Their Enantiopreference, and Prospects for Mirror-Image Biotransformations. *Angew. Chemie - Int. Ed.* **2008**, *47* (46), 8782–8793.

(28) Tufvesson, P.; Lima-Ramos, J.; Jensen, J. S.; Al-Haque, N.; Neto, W.; Woodley, J. M. Process Considerations for the Asymmetric Synthesis of Chiral Amines Using Transaminases. *Biotechnol. Bioeng.* **2011**, *108* (7), 1479–1493.

(29) Tufvesson, P.; Jensen, J. S.; Kroutil, W.; Woodley, J. M. Experimental Determination of Thermodynamic Equilibrium in Biocatalytic Transamination. *Biotechnol. Bioeng.* **2012**, *109* (8), 2159–2162.

(30) Kelefiotis-Stratidakis, P.; Tyrikos-Ergas, T.; Pavlidis, I. V. The Challenge of Using Isopropylamine as an Amine Donor in Transaminase Catalysed Reactions. *Org. Biomol. Chem.* **2019**, *17* (7), 1634–1642.

(31) Koszelewski, D.; Lavandera, I.; Clay, D.; Rozzell, D.; Kroutil, W. Asymmetric Synthesis of Optically Pure Pharmacologically Relevant Amines Employing ω-Transaminases. *Adv. Synth. Catal.* **2008**, *350* (17), 2761–2766.

(32) Höhne, M.; Kühl, S.; Robins, K.; Bornscheuer, U. T. Efficient Asymmetric Synthesis of Chiral Amines by Combining Transaminase and Pyruvate Decarboxylase. *ChemBioChem* **2008**, *9* (3), 363–365.

(33) Satyawali, Y.; del Pozo, D. F.; Vandezande, P.; Nopens, I.; Dejonghe, W. Investigating

Pervaporation for in Situ Acetone Removal as Process Intensification Tool in ω-Transaminase Catalyzed Chiral Amine Synthesis. *Biotechnol. Prog.* **2019**, *35* (1).

(34) Martínez-Montero, L.; Gotor, V.; Gotor-Fernández, V.; Lavandera, I. But-2-Ene-1,4-Diamine and But-2-Ene-1,4-Diol as Donors for Thermodynamically Favored Transaminase- and Alcohol Dehydrogenase-Catalyzed Processes. *Adv. Synth. Catal.* **2016**, *358* (10), 1618–1624.

(35) Green, A. P.; Turner, N. J.; O'Reilly, E. Chiral Amine Synthesis Using ω-Transaminases: An Amine Donor That Displaces Equilibria and Enables High-Throughput Screening. *Angew. Chemie - Int. Ed.* **2014**, *53* (40), 10714–10717.

(36) Gomm, A. A.; Lewis, W.; Green, A. P.; Reilly, E. O.; Gomm, A.; Lewis, W.; Green, A. P.; Reilly, E. O. A New Generation of Smart Amine Donors for Transaminase- Mediated Biotransformations. *Chem. Eur. J.* **2016**, *22* (36), 12692–12695.

(37) Asimov, I. Enzymes and Metaphor. *J. Chem. Educ.* **1959**, *36*, 535–538.

(38) Savile, C. K.; Janey, J. M.; Mundorff, E. C.; Moore, J. C.; Tam, S.; Jarvis, W. R.; Colbeck, J. C.; Krebber, A.; Fleitz, F. J.; Brands, J.; Devine, P. N.; Huisman, G. W.; Hughes, G. J. Biocatalytic Asymmetric Synthesis of Chiral Amines from Ketones Applied to Sitagliptin Manufacture. *Science.* **2010**, *329* (5989), 305–309.

(39) Jia, D. X.; Peng, C.; Li, J. L.; Wang, F.; Liu, Z. Q.; Zheng, Y. G. Redesign of (R)-Omega-Transaminase and Its Application for Synthesizing Amino Acids with Bulky Side Chain. *Appl. Biochem. Biotechnol.* **2021**, *193* (11), 3624–3640.

(40) Gao, X.; Zhang, X.; Zhu, N.; Mou, Y.; Zhang, H.; Liu, X.; Wei, P. Reshaping the Substrate Binding Region of (R)-Selective ω-Transaminase for Asymmetric Synthesis of (R)-3-Amino-1-Butanol. *Appl. Microbiol. Biotechnol.* **2020**, *104* (9), 3959–3969.

(41) Park, E. S.; Park, S. R.; Han, S. W.; Dong, J. Y.; Shin, J. S. Structural Determinants for the Non-Canonical Substrate Specificity of the ω-Transaminase from Paracoccus Denitrificans. *Adv. Synth. Catal.* **2014**, *356* (1), 212–220.

(42) Scheib, H.; Pleiss, J.; Stadler, P.; Kovac, A.; Potthoff, A. P.; Haalck, L.; Spener, F.; Paltauf, F.; Schmid, R. D. Rational Design of Rhizopus Oryzae Lipase with Modified Stereoselectivity toward Triradylglycerols. *Protein Eng.* **1998**, *11* (8), 675–682.

(43) Chen, V. B.; Arendall, W. B.; Headd, J. J.; Keedy, D. A.; Immormino, R. M.; Kapral, G. J.; Murray, L. W.; Richardson, J. S.; Richardson, D. C. MolProbity: All-Atom Structure Validation for Macromolecular Crystallography. *Acta Crystallogr. Sect. D Biol. Crystallogr.* **2010**, *66* (1), 12–21.

(44) Kibbe, W. A. OligoCalc: An Online Oligonucleotide Properties Calculator. *Nucleic Acids Res.* **2007**, *35*, 43–46.

(45) Schätzle, S.; Höhne, M.; Redestad, E.; Robins, K.; Bornscheuer, U. T. Rapid and Sensitive Kinetic Assay for Characterization of ω-Transaminases. *Anal. Chem.* **2009**, *81* (19), 8244–8248.

(46) Voss, M.; Xiang, C.; Esque, J.; Nobili, A.; Menke, M. J.; André, I.; Höhne, M.; Bornscheuer, U. T. Creation of (R)-Amine Transaminase Activity within an α-Amino Acid Transaminase Scaffold. *ACS Chem. Biol.* **2020**, *15* (2), 416–424.

(47) Pearl, F. M. G.; Bennett, C. F.; Bray, J. E.; Harrison, A. P.; Martin, N.; Shepherd, A.; Sillitoe, I.; Thornton, J.; Orengo, C. A. The CATH Database: An Extended Protein Family Resource for Structural and Functional Genomics. *Nucleic Acids Res.* **2003**, *31* (1), 452–455.

(48) Chaput, L.; Sanejouand, Y. H.; Balloumi, A.; Tran, V.; Graber, M. Contribution of Both Catalytic Constant and Michaelis Constant to CALB Enantioselectivity: Use of FEP Calculations for Prediction Studies. *J. Mol. Catal. B Enzym.* **2012**, *76*, 29–36.

(49) Han, S. W.; Park, E. S.; Dong, J. Y.; Shin, J. S. Mechanism-Guided Engineering of ω-

Transaminase to Accelerate Reductive Amination of Ketones. *Adv. Synth. Catal.* **2015**, *357* (8), 1732–1740.

(50) Han, S. W.; Park, E. S.; Dong, J. Y.; Shin, J. S. Expanding Substrate Specificity of ω-Transaminase by Rational Remodeling of a Large Substrate-Binding Pocket. *Adv. Synth. Catal.* **2015**, *357* (12), 2712–2720.

(51) Meng, Q.; Ramírez-Palacios, C.; Capra, N.; Hooghwinkel, M. E.; Thallmair, S.; Rozeboom, H. J.; Thunnissen, A. M. W. H.; Wijma, H. J.; Marrink, S. J.; Janssen, D. B. Computational Redesign of an ω-Transaminase FromPseudomonas Jesseniifor Asymmetric Synthesis of Enantiopure Bulky Amines. *ACS Catal.* **2021**, *11* (17), 10733–10747.

(52) Bezsudnova, E. Y.; Boyko, K. M.; Popov, V. O. Properties of Bacterial and Archaeal Branched-Chain Amino Acid Aminotransferases. *Biochem.* **2017**, *82* (13), 1572–1591.

(53) Limbach, H.; Chan-huot, M.; Sharif, S.; Tolstoy, P. M.; Shenderovich, I. G.; Denisov, G. S.; Toney, M. D. Critical Hydrogen Bonds and Protonation States of Pyridoxal 5′-Phosphate Revealed by NMR. *Biochim. Biophys. Acta* **2011**, *1814*, 1419–1425.

(54) Passera, E.; Campanini, B.; Rossi, F.; Casazza, V.; Rizzi, M.; Pellicciari, R.; Mozzarelli, A. Human Kynurenine Aminotransferase II - Reactivity with Substrates and Inhibitors. *FEBS J.* **2011**, *278* (11), 1882–1900.

(55) Rojas-Ortega, E.; Aguirre-López, B.; Reyes-Vivas, H.; González-Andrade, M.; Campero-Basaldúa, J. C.; Pardo, J. P.; González, A. Saccharomyces Cerevisiae Differential Functionalization of Presumed ScALT1 and ScALT2 Alanine Transaminases Has Been Driven by Diversification of Pyridoxal Phosphate Interactions. *Front. Microbiol.* **2018**, *9*, 1–16.

(56) Shin, J. S.; Yun, H.; Jang, J. W.; Park, I.; Kim, B. G. Purification, Characterization, and Molecular Cloning of a Novel Amine:Pyruvate Transaminase from Vibrio Fluvialis JS17. *Appl. Microbiol. Biotechnol.* **2003**.

(57) Vázquez, M. A.; Muñoz, F.; Donoso, J.; García Blanco, F. Stability of Schiff Bases of Amino Acids and Pyridoxal-5'-Phosphate. *Amino Acids* **1992**, *3* (1), 81–94.